JOURNAL OF GEOPHYSICAL RESEARCH, VOL. 111, D12304, doi:10.1029/2005JD006852, 2006

Role of climate change in global predictions of future tropospheric ozone and aerosols

Hong Liao,[1] Wei-Ting Chen,[1] and John H. Seinfeld[1,2]

Received 4 November 2005; revised 1 February 2006; accepted 1 March 2006; published 17 June 2006.

[1] A unified tropospheric chemistry-aerosol model within the Goddard Institute for Space Studies general circulation model II′ is applied to simulate an equilibrium CO_2-forced climate in the year 2100 to examine the effects of climate change on global distributions of tropospheric ozone and sulfate, nitrate, ammonium, black carbon, primary organic carbon, secondary organic carbon, sea salt, and mineral dust aerosols. The year 2100 CO_2 concentration as well as the anthropogenic emissions of ozone precursors and aerosols/aerosol precursors are based on the Intergovernmental Panel on Climate Change Special Report on Emissions Scenarios (SRES) A2. Year 2100 global O_3 and aerosol burdens predicted with changes in both climate and emissions are generally 5–20% lower than those simulated with changes in emissions alone; as exceptions, the nitrate burden is 38% lower, and the secondary organic aerosol burden is 17% higher. Although the CO_2-driven climate change alone is predicted to reduce the global O_3 burden as a result of faster removal of O_3 in a warmer climate, it is predicted to increase surface layer O_3 concentrations over or near populated and biomass burning areas because of slower transport, enhanced biogenic hydrocarbon emissions, decomposition of peroxyacetyl nitrate at higher temperatures, and the increase of O_3 production by increased water vapor at high NO_x levels. The warmer climate influences aerosol burdens by increasing aerosol wet deposition, altering climate-sensitive emissions, and shifting aerosol thermodynamic equilibrium. Climate change affects the estimates of the year 2100 direct radiative forcing as a result of the climate-induced changes in burdens and different climatological conditions; with full gas-aerosol coupling and accounting for ozone and aerosols from both natural and anthropogenic sources, year 2100 global mean top of the atmosphere direct radiative forcings by O_3, sulfate, nitrate, black carbon, and organic carbon are predicted to be +0.93, −0.72, −1.0, +1.26, and −0.56 W m^{-2}, respectively, using present-day climate and year 2100 emissions, while they are predicted to be +0.76, −0.72, −0.74, +0.97, and −0.58 W m^{-2}, respectively, with year 2100 climate and emissions.

Citation: Liao, H., W.-T. Chen, and J. H. Seinfeld (2006), Role of climate change in global predictions of future tropospheric ozone and aerosols, *J. Geophys. Res.*, *111*, D12304, doi:10.1029/2005JD006852.

1. Introduction

[2] Tropospheric O_3 and aerosols have made important contributions to radiative forcing since preindustrial times [*Intergovernmental Panel on Climate Change* (*IPCC*), 2001] and are predicted to do so in the future. Their abundances are controlled by a combination of direct and precursor emissions, chemical reactions in the atmosphere, and meteorological processes, all of which can be significantly affected by climate change with resulting feedbacks. Tropospheric O_3 and aerosols have relatively short atmospheric lifetimes (days to weeks) and hence inhomogeneous atmospheric distributions, complicating the link between radiative forcing and climate response [*Hansen et al.*, 1997].

[3] Climate change influences tropospheric ozone and aerosols through effects on emissions, transport, and atmospheric chemistry. Biogenic emissions of NO_x and hydrocarbons [*Atherton et al.*, 1995; *Yienger and Levy*, 1995; *Guenther et al.*, 1995; *Constable et al.*, 1999] are sensitive to temperature. Increasing deep convection enhances the lightning NO_x source [*Toumi et al.*, 1996; *Sinha and Toumi*, 1997]. Changes in surface winds have impacts on emissions of dimethylsulfide (DMS) [*Bopp et al.*, 2004], sea salt, and mineral dust. The potential impacts of climate change on transport of ozone and aerosols have been demonstrated by general circulation model (GCM) studies. *Rind et al.* [2001] predicted that increased convection in a doubled-CO_2 atmosphere leads to improved ventilation of the lowest layers of the atmosphere, reducing boundary layer concentrations of tracers. *Holzer and Boer* [2001] reported that if a warmer climate leads to weaker winds, higher tracer concentrations will exist in the vicinity of sources. Changes in boundary

[1]Department of Environmental Science and Engineering, California Institute of Technology, Pasadena, California, USA.
[2]Department of Chemical Engineering, California Institute of Technology, Pasadena, California, USA.

0148-0227/06/2005JD006852$09.00

layer conditions and hydrological cycle influence overall dry and wet deposition. Furthermore, chemical reaction rates are influenced by changes in atmospheric water vapor and temperature.

[4] The effects of climate change on tropospheric ozone have been simulated in several global studies. On the basis of the doubled CO_2 climate predicted by the NCAR CCM and projected year 2050 ozone precursor emissions from the IS92a scenario, *Brasseur et al.* [1998] predicted a 7% increase in the global mean OH abundance and a 5% decrease in O_3 in the tropical upper troposphere relative to current climate. In offline chemistry simulations, *Johnson et al.* [1999] predicted that a doubled CO_2 climate with precursor emissions kept at present-day levels would reduce the tropospheric ozone burden by about 10%. Coupled chemistry-GCM simulations by *Johnson et al.* [2001] predicted that with projected precursor emissions over 1990–2100, the global burden of O_3 calculated with simulated 2100 climate would be lower than that predicted with present-day climate. These studies concluded that higher temperature and water vapor content in a warmer climate would lead to the reduction in global O_3.

[5] No study has systematically addressed the effect of climate change on future global aerosol concentrations. Previous global projections of future aerosol levels have generally simulated concentrations on the basis of present-day climate and accounted only for projected changes in emissions [*Adams et al.*, 2001; *Koch*, 2001; *Iversen and Seland*, 2002; *Liao and Seinfeld*, 2005]; also, present-day gas-phase oxidant concentrations were used for future aerosol simulations [*Adams et al.*, 2001; *Koch*, 2001; *Iversen and Seland*, 2002].

[6] We examine here the changes in global concentrations of ozone, sulfate, nitrate, ammonium, black carbon, primary organic carbon, secondary organic carbon, sea salt, and mineral dust aerosols over the period 2000–2100 using a unified tropospheric chemistry-aerosol model within the Goddard Institute for Space Studies (GISS) GCM II′. We first predict equilibrium climate change resulting from projected changes in CO_2 over 2000–2100, then examine the effect of CO_2-induced climate change on abundances of ozone and aerosols at present-day anthropogenic emissions levels, and finally estimate the O_3 and aerosol levels in 2100 corresponding to the combined effects of both climate change and changes in emissions. The ozone and aerosol simulations account for the coupling between aerosols and gas-phase chemistry. Heterogeneous reactions on aerosols affect the concentrations of HO_x, NO_x, and O_3. In addition, aerosols affect gas-phase photolysis rates, and climate change influences natural emissions of NO_x, hydrocarbons, DMS, sea salt, and mineral dust. Full simulation of gas-phase chemistry and aerosols provides consistent chemical species for both present-day and future scenarios.

[7] *Liao and Seinfeld* [2005] estimated year 2100 radiative forcing by tropospheric ozone and aerosols based on present-day climate. With coupled climate, chemistry, and aerosols, we also examine here the effect of climate change on estimates of future radiative forcing. The model description and experimental design are given in section 2. Section 3 presents the simulated climate change over 2000–2100. The impact of climate change alone on the predictions of O_3 and aerosols is then examined in section 4. Section 5 presents the changes in ozone and aerosol concentrations over 2000–2100 simulated with both predicted climate change and projected emissions. In section 6, we examine the effect of climate change on estimates of year 2100 direct radiative forcing by O_3 and aerosols.

2. Model Description and Experimental Design

2.1. Unified Model

[8] The simulations in this work are performed using the unified model reported by *Liao et al.* [2003, 2004] and *Liao and Seinfeld* [2005], which is a fully coupled chemistry-aerosol-climate GCM with tropospheric O_3-NO_x-hydrocarbon chemistry and sulfate/nitrate/ammonium/sea-salt/water, black carbon, primary organic carbon, secondary organic carbon, and mineral dust aerosols within the Goddard Institute for Space Studies (GISS) GCM II′ [*Rind and Lerner*, 1996; *Rind et al.*, 1999]. The GCM has a resolution of 4° latitude by 5° longitude, with 9 vertical layers in a σ-coordinate system extending from the surface to 10 mbar. The chemical mechanism includes 225 chemical species and 346 reactions for simulating gas-phase species and aerosols. Tracers that describe O_3-NO_x-hydrocarbon chemistry include odd oxygen ($O_x = O_3 + O + NO_2 + 2NO_3$), NO_x ($NO + NO_2 + NO_3 + HNO_2$), N_2O_5, HNO_3, HNO_4, peroxyacetyl nitrate, H_2O_2, CO, C_3H_8, C_2H_6, ($\geq C_4$) alkanes, ($\geq C_3$) alkenes, isoprene, acetone, CH_2O, CH_3CHO, CH_3OOH, ($\geq C_3$) aldehydes, ($\geq C_4$) ketones, methyl vinyl ketone, methacrolein, peroxymethacryloyl nitrate, lumped peroxyacyl nitrates, and lumped alkyl nitrates. Aerosol related tracers include SO_2, SO_4^{2-}, dimethyl sulfide (DMS), NH_3, NH_4^+, NO_3^-, sea salt in 11 size bins (0.031–0.063, 0.063–0.13, 0.13–0.25, 0.25–0.5, 0.5–1, 1–2, 2–4, 4–8, 8–16, 16–32, 32–64 μm dry radius), mineral dust in 6 size bins (0.0316–0.1, 0.1–0.316, 0.316–1.0, 1.0–3.16, 3.16–10, and 10–31.6 μm dry radius), black carbon (BC), primary organic aerosol (POA), as well as 5 classes of reactive hydrocarbons and 28 organic oxidation products involved in secondary organic aerosol (SOA) formation. The partitioning of ammonia and nitrate between gas and aerosol phases is determined by the on-line thermodynamic equilibrium model ISORROPIA [*Nenes et al.*, 1998], and the formation of secondary organic aerosol is based on equilibrium partitioning and experimentally determined yield parameters [*Griffin et al.*, 1999a, 1999b; *Chung and Seinfeld*, 2002]. Two-way coupling between aerosols and gas-phase chemistry provides consistent chemical fields for aerosol dynamics and aerosol mass for heterogeneous processes and calculations of gas-phase photolysis rates. Heterogeneous reactions considered in the model include those of N_2O_5, NO_3, NO_2, and HO_2 on wet aerosols, uptake of SO_2 by sea salt, and uptake of SO_2, HNO_3 and O_3 by mineral dust; the uptake coefficients are taken to depend on atmospheric temperature and relative humidity, as described by *Liao and Seinfeld* [2005].

[9] Dry and wet deposition schemes for tracers are described by *Liao et al.* [2003, 2004]. For the purpose of this study, we have updated the dry deposition velocities used for carbonaceous aerosols. In the studies of *Liao et al.* [2003, 2004] and *Liao and Seinfeld* [2005], a fixed deposition velocity of 0.1 cm s^{-1} was used for black carbon, primary organic carbon, and secondary organic carbon aerosols following the studies of *Liousse et al.* [1996],

Kanakidou et al. [2000], and *Chung and Seinfeld* [2002]. To account for possible effects of climate change on dry deposition, dry deposition velocities of carbonaceous aerosols are determined using the resistance-in-series scheme of *Wesely* [1989], which has been used for dry deposition of other aerosol species [*Liao et al.*, 2003].

2.2. Climate Simulations

[10] We perform two simulations of equilibrium climate using the unified model, one for year 2000 with a CO_2 concentration of 368 ppmv and the other for year 2100 with a CO_2 concentration of 836 ppmv, based on IPCC Special Report on Emissions Scenarios (SRES) A2 [*IPCC*, 2001]. Of the IPCC scenarios characterized by different socioeconomic assumptions, the SRES A2 has the highest growth of emissions. The settings of these two simulations, except for the CO_2 concentration, are identical, each with a q-flux ocean [*Hansen et al.*, 1984; *Russell et al.*, 1984]. In the q-flux ocean, ocean heat transport is held constant but sea surface temperatures and ocean ice respond to changes in climate. The monthly mean ocean heat transport fluxes are from the work of *Mickley et al.* [2004], which used the same version of the GCM as here to generate observed, present-day sea surface temperatures. In these two climate simulations, present-day climatological aerosol and ozone concentrations are used in the GCM radiative calculations to isolate the climate change driven by the change in CO_2 concentration. Each climate simulation is integrated for 50 years to allow the climate to reach an equilibrium state, and the simulated climate over years 50–55 is used to drive the chemistry simulations described in section 2.3.

[11] Because future emissions scenarios are, of course, uncertain, we have chosen here to consider a future greenhouse climate as driven by CO_2 only and, as noted, have applied IPCC SRES A2. Future climate will be influenced in addition by changes in CH_4, N_2O, and CFCs, but these species need not be included here, as CO_2 under SRES A2 provides ample climate change to examine the effects of climate-chemistry-aerosol coupling.

[12] Traditionally, climate simulations take one of two forms: (1) equilibrium climate, in which the long-term climate that would result from a fixed greenhouse gas concentration is computed; and (2) transient climate, in which climate is simulated from a starting point, say preindustrial, with specified annual emissions changes. Predicted changes from an equilibrium climate simulation generally exceed those from a transient climate simulation. For example, the ratio of transient climate response (the change in surface air temperature at the time of doubled CO_2) to the equilibrium response (the equilibrium change in surface air temperature from doubled CO_2) lies in the range of 0.47–0.68 [*IPCC*, 1995; *Kiehl et al.*, 2006]. Although non-CO_2 greenhouse gases are not included in the present year 2100 equilibrium climate simulation, the predicted climate responses are comparable to or slightly larger than those predicted from a transient climate simulation driven by the changes in all greenhouse gases over 2000–2100. Hereafter for convenience we refer to the simulated CO_2-driven equilibrium climate as year 2000 or 2100 climate, but we note that the CO_2-driven equilibrium climate differs from a transient climate including all greenhouse gases and aerosols, as discussed above.

2.3. Chemistry Simulations

[13] Chemistry simulations are performed when the climate simulations reach equilibrium states. The simulated climates over years 50–55 drive the chemistry simulations, with the first year of each chemistry simulation considered spin up. Four chemistry simulations are designed to identify the effects of climate change on levels of tropospheric ozone and aerosols (Table 1):

[14] 1. CL2000EM2000 is the control simulation with the year 2000 climate and present-day (approximately year 2000) anthropogenic emissions of ozone precursors and aerosols/aerosol precursors (non-CO_2 anthropogenic emissions).

[15] 2. CL2100EM2000 is the simulation with year 2100 CO_2-driven climate and present-day non-CO_2 anthropogenic emissions.

[16] 3. CL2000EM2100 is the simulation with year 2000 climate and year 2100 non-CO_2 anthropogenic emissions.

[17] 4. CL2100EM2100 uses year 2100 CO_2-driven climate and year 2100 non-CO_2 anthropogenic emissions.

[18] Climate-sensitive natural emissions are calculated on the basis of predicted climate in all the simulations (section 2.4). By holding non-CO_2 anthropogenic emissions at present-day levels, the difference between CL2100EM2000 and CL2000EM2000 reflects the effects of CO_2-driven climate change alone on concentrations of O_3 and aerosols. The difference between CL2100EM2100 and CL2000EM2000 represents the impacts of both climate and emission changes on O_3 and aerosol levels. CL2000EM2100 uses present-day climate and year 2100 anthropogenic emissions, in a manner used in a number of previous studies, to predict future O_3 and aerosols. We will compare the radiative forcings calculated in CL2000EM2100 and CL2100EM2100 to examine the effect of climate change on radiative forcing.

[19] Heterogeneous reactions have been shown to be potentially influential in coupling processes involving O_3 and aerosols [*Liao and Seinfeld*, 2005]. In the present study we perform each of the four chemistry simulations, CL2100EM2000, CL2000EM2000, CL2000EM2100, and CL2100EM2100, in the absence and presence of heterogeneous reactions of N_2O_5, NO_3, NO_2, and HO_2 on wet aerosols, uptake of SO_2 by sea salt, and the uptake of SO_2, HNO_3 and O_3 by mineral dust. The simulations that include heterogeneous reactions will be designated as CL2100EM2000h, CL2000EM2000h, CL2000EM2100h, and CL2100EM2100h. Uptake coefficients for heterogeneous reactions are given by *Liao and Seinfeld* [2005]. The chemistry simulations performed are summarized in Table 1.

[20] Unless otherwise noted, the annual, seasonal, or monthly chemical fields presented in this work are averaged over the last 5 years of each chemistry simulation, and the meteorological fields are averaged over years 51–55 of each climate simulation. The climate-chemistry coupling is one-way; simulated O_3 and aerosols do not feed back into the GCM.

2.4. Emission Inventories

[21] Present-day and year 2100 non-CO_2 anthropogenic emissions used in the chemistry simulations are given in

Table 1. Summary of Chemistry Simulations[a]

Experiments	CO_2 Mixing Ratio, ppmv	Nominal Year of GCM Climate	Non-CO_2 Anthropogenic Emissions	Heterogeneous Reactions
CL2000EM2000	368	2000	present day	no
CL2000EM2000h	368	2000	present day	yes
CL2100EM2000	836	2100	present day	no
CL2100EM2000h	836	2100	present day	yes
CL2000EM2100	368	2000	2100	no
CL2000EM2100h	368	2000	2100	yes
CL2100EM2100	836	2100	2100	no
CL2100EM2100h	836	2100	2100	yes

[a]Climate-sensitive natural emissions depend on the simulated climate in all the simulations. See Table 3 for details.

Table 2. Year 2100 anthropogenic emissions are based on the IPCC SRES A2 emissions scenario. Biomass burning emissions listed in Table 2 are partly anthropogenic and partly natural. We assume in this study that the biomass burning emissions remain unchanged in 2000 and 2100 simulations; the effect of climate change on the occurrence and intensity of wildfires is not considered. The seasonal and geographical distributions of BC and POA emissions in year 2100 are obtained by scaling year 2000 monthly values, grid by grid, using projected changes in IPCC SRES A2 CO emissions.

[22] Climate-sensitive natural emissions include lightning NO_x, NO_x from soil, biogenic hydrocarbons, DMS, sea salt, and mineral dust. The meteorological variables that influence these emissions and the schemes used to predict them are listed in Table 3. Emissions of biogenic hydrocarbons and mineral dust are calculated on the basis of fixed distributions of land-surface type and vegetation. We calculate the global monoterpene emissions as a function of vegetation type, monthly adjusted leaf area index, and model predicted temperature, using the base monoterpene emission flux and the formulation of *Guenther et al.* [1995]. The vegetation type and the calculation of leaf area index follow the treatment by *Wang et al.* [1998]. Predicted present-day total monoterpene emissions of 117 TgC yr^{-1} agree reasonably well with the 127 TgC yr^{-1} reported by *Guenther et al.* [1995]. For present-day emission inventories of other reactive volatile organic compounds (ORVOCs), we use the offline monthly fields from the Global Emissions Inventory Activity (GEIA), but year 2100 emissions of ORVOCs in a grid cell are scaled by the monthly mean ratio of year 2100 emissions to the year 2000 values predicted for monoterpenes. Representation of future isoprene emissions is similar to the approach used for future monoterpenes and follows the algorithm of *Guenther et al.* [1995], which considers immediate light and temperature dependence but does not account for the suppression of isoprene emissions under elevated ambient CO_2 concentrations [*Rosenstiel et al.*, 2003] and the acclimation of plants to higher temperatures [*P'etron et al.*, 2001]. In all chemistry simulations, transport of ozone from the stratosphere is held fixed at 401 Tg O_3 yr^{-1}.

3. Predicted Climate Change

[23] In this section, we briefly summarize the changes in meteorological fields over the period 2000–2100 based on

Table 2. Global Annual Anthropogenic Emissions for the Years 2000 and 2100

Species	Present-Day 2000 Scenario	IPCC SRES A2 2100 Scenario
NO_x,[a] Tg N yr^{-1}		
Fossil fuel combustion	20	96
Biomass burning	11	11
Soil (fertilizer)	0.5	0.5
Aircraft	0.5	2.2
Total	32	109.7
CO,[a] Tg CO yr^{-1}		
Fossil fuel combustion	390	1858
Wood fuel combustion	130	130
Biomass burning	510	510
Total	1030	2498
Ethane,[a] Tg C yr^{-1}		
Industrial	6.2	97.7
Biomass burning	2.4	2.4
Total	8.6	100.1
Propane,[a] Tg C yr^{-1}		
Industrial	6.7	28.1
$\geq C_4$ alkanes,[a] Tg C yr^{-1}		
Industrial	30.1	60.5
$\geq C_3$ alkenes,[a] Tg C yr^{-1}		
Industrial	10	29
Biomass burning	12	12
Total	22	41
Acetone,[a] Tg C yr^{-1}		
Biomass burning	9	9
SO_2, Tg S yr^{-1}		
Industrial	69	60.3
Biomass burning	2.3	2.3
Total	71.3	62.6
NH_3,[b] Tg N yr^{-1}		
Agricultural	37.4	88.8
Biomass burning	6.4	6.4
Other	3.1	7.4
Total	46.9	102.6
POA, Tg OM yr^{-1}		
Biomass burning	54	
Fossil fuel	28.2	
Total	82.2[c]	189.5[e]
BC, Tg C yr^{-1}		
Biomass burning	5.6	
Fossil fuel	6.6	
Total	12.2[c,d]	28.8[e]

[a]*Mickley et al.* [1999]; *Gauss et al.* [2003].
[b]*Bouwman et al.* [1997]; *Adams et al.* [2001]. Natural NH_3 emissions from oceans, undisturbed soils, and wild animals are assumed to be 10.7 Tg N yr^{-1} in both 2000 and 2100 simulations.
[c]*Liousse et al.* [1996].
[d]*Penner et al.* [1993].
[e]Scaled to projected changes in CO.

Table 3. Climate-Sensitive Natural Emissions

Species	GCM Variables That Influence Emissions	Emission Schemes	Year 2000 Predicted Emissions	Year 2100 Predicted Emissions
NO_x from soil	temperature, precipitation	*Wang et al.* [1998]	4.5 Tg N yr^{-1}	5.6 Tg N yr^{-1}
NO_x from lightning	frequency of convective events	*Wang et al.* [1998]	3.3 Tg N yr^{-1}	4.0 Tg N yr^{-1}
Isoprene	temperature, solar radiation	*Guenther et al.* [1995]; *Wang et al.* [1998]	437.9 Tg C yr^{-1}	680.4 Tg C yr^{-1}
Biogenic acetone	temperature, solar radiation	*Wang et al.* [1998]	10.9 Tg C yr^{-1}	17.0 Tg C yr^{-1}
Biogenic $\geq C_3$ alkenes	temperature, solar radiation	*Wang et al.* [1998]	12.5 Tg C yr^{-1}	19.5 Tg C yr^{-1}
Monoterpenes	temperature, solar radiation	*Guenther et al.* [1995]; *Wang et al.* [1998]	117 Tg C yr^{-1}	185 Tg C yr^{-1}
ORVOCs	temperature, solar radiation	see section 2.4	260 Tg C yr^{-}	411 Tg C yr^{-1}
DMS	Surface wind, temperature	*Kettle et al.* [1999]; *Liss and Merlivat* [1986]	22.5 Tg S yr^{-1}	24.9 Tg S yr^{-1}
Sea salt	wind	*Monahan et al.* [1986]; *Smith and Harrison* [1998]; *Liao et al.* [2004]	6314.2 Tg yr^{-1}	5947.8 Tg yr^{-1}
Mineral dust	wind, soil moisture	*Gillette* [1978]; *Liao et al.* [2004]	1816.9 Tg yr^{-1}	1567.6 Tg yr^{-1}

the two equilibrium CO_2-driven climate simulations described above.

3.1. Predicted Changes in Temperature

[24] Predicted changes in surface and zonal mean atmospheric temperature over 2000–2100 as a result of the increase in CO_2 mixing ratio from 368 ppmv to 836 ppmv are shown in Figures 1a and 1b. Annual average surface air temperature is predicted to increase by 4.8°C. Doubling CO_2 relative to the present-day yields a climate sensitivity of 0.8°C m^2 W^{-1}, a value that lies within the range of sensitivity reported for current GCMs [*Ramaswamy*, 2001; *Hansen et al.*, 1997]. Predicted zonal mean changes in atmospheric temperature exhibit the same pattern as those summarized by *IPCC* [2001]. Enhanced warming in the tropical mid to upper troposphere results from enhanced latent heating owing to more vigorous moist convection in a warmer climate [*Hansen et al.*, 1984; *Mitchell*, 1989] and from increased longwave radiative heating when upper tropospheric cloudiness and water vapor increase with temperature [*Dai et al.*, 2001]. The strong warming predicted in the high latitudes of the Northern Hemisphere is a result of sea-ice climate feedback.

3.2. Predicted Changes in Hydrological Cycle

[25] Figure 2a shows predicted year 2000 zonal annual mean specific humidity (g H_2O/kg air) as a function of pressure. The predicted distribution of specific humidity is similar to that from the NCEP–NCAR reanalysis [*Kalnay et al.*, 1996]. As air temperature rises over 2000–2100, specific humidity is predicted to generally increase, with the largest increases of 3–4.5 g H_2O/kg air located in the lower troposphere (below 800 mb) over the low latitudes (Figure 2b), because of the nonlinear temperature dependence of the Clausius–Clapeyron equation. The predicted pattern of changes in specific humidity is similar to that predicted in other GCM simulations [*IPCC*, 1995; *Dai et al.*, 2001].

[26] The predicted change in global mean precipitation is +0.32 mm day^{-1} over 2000–2100 (Figure 2c), a 10% increase from the global mean value predicted for year 2000. Precipitation increases over middle to high latitudes in both hemispheres, associated with the large warming at the surface and in the lower troposphere [*Dai et al.*, 2001]. Reductions in precipitation are predicted over tropics and subtropics, which are associated with the predicted weakening of the Hadley circulation, as discussed below. Zonal mean precipitation increases (Figure 2d) at all latitudes except around 20°S, which agrees qualitatively with the changes from the 1990s to the 2090s simulated by *Dai et al.* [2001] using the NCAR GCM. Increases in precipitation are predicted over North Africa, changes that are consistent with the predictions of other GCMs [*IPCC*, 2001, chap. 9.3.2,]; these will influence mineral dust emissions, as discussed subsequently.

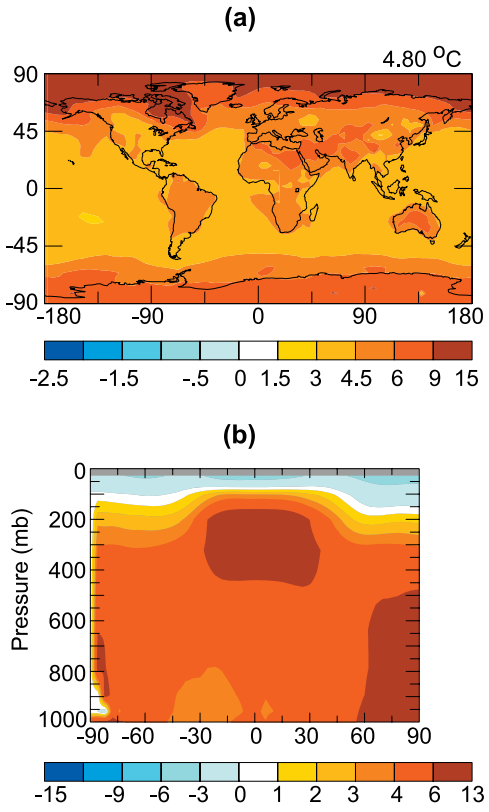

Figure 1. Temperature responses in the equilibrium climate to the increase in CO_2 concentration from 368 ppmv in year 2000 to 836 ppmv in year 2100, including predicted changes (°C) in (a) annual mean surface air temperature and (b) zonal annual mean atmospheric temperature. The global mean value is indicated at the top right corner of Figure 1a.

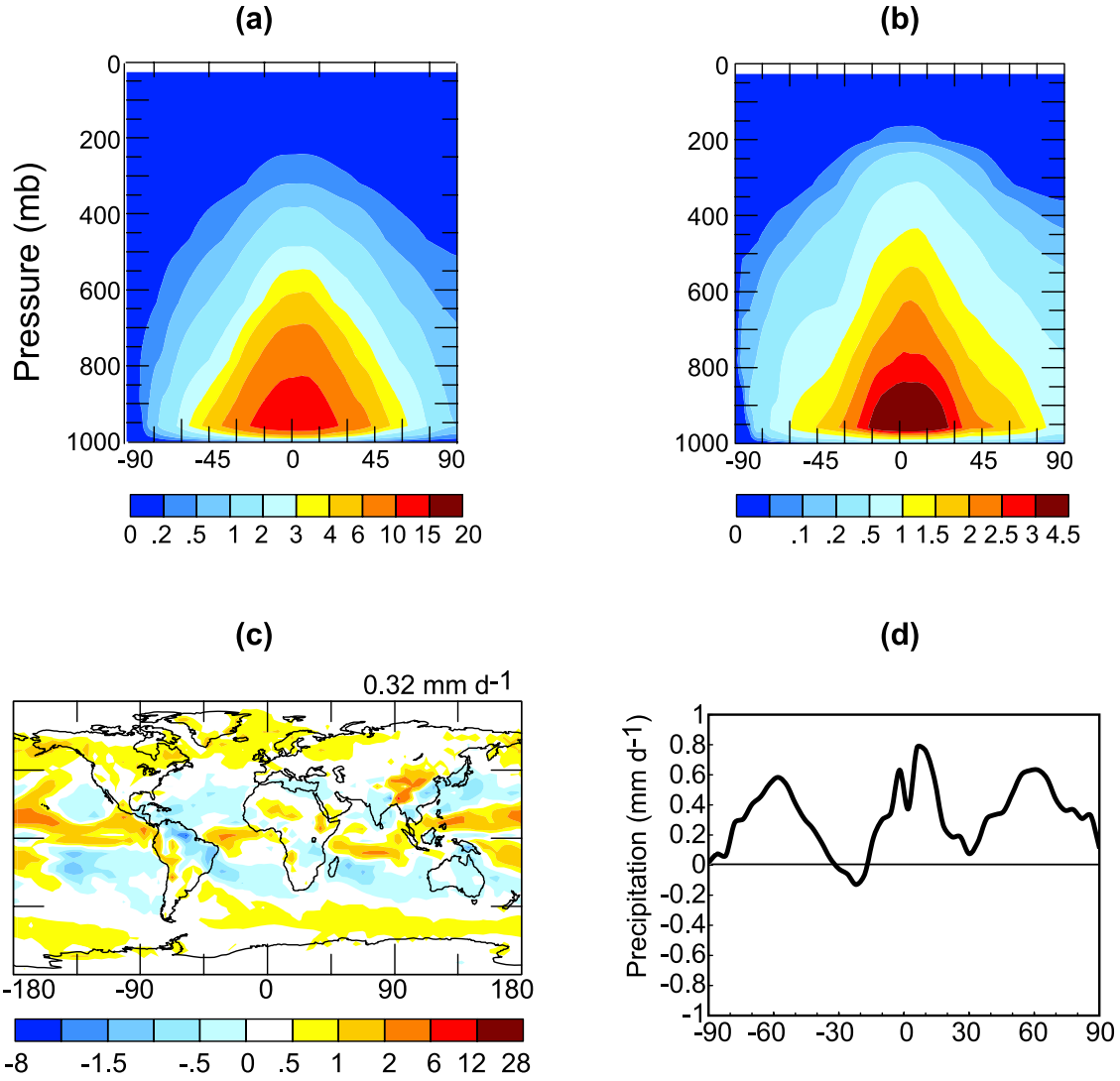

Figure 2. (a) Predicted year 2000 zonal annual mean equilibrium specific humidity (g H_2O/kg air) as a function of pressure. (b) Predicted changes in zonal annual mean equilibrium specific humidity (g H_2O/kg air) relative to year 2000. (c) Predicted changes (mm d^{-1}) relative to year 2000 in annual mean precipitation. (d) Predicted changes (mm d^{-1}) relative to year 2000 in zonal annual mean precipitation. The global mean value is indicated at the top right corner of Figure 2c.

3.3. Predicted Changes in Winds

[27] Enhanced warming at the high latitudes in both hemispheres and changes in the vertical temperature profiles (Figures 1a and 1b) lead to changes in atmospheric circulation. Figures 3a and 3b show the predicted zonal and seasonal mean distributions of the present-day vertical velocity and the changes in vertical velocity from year 2000 to year 2100, respectively. The most obvious effect shown in Figure 3 is the weakening of the Hadley cells in both hemispheres. The ascending branches of the Hadley cells are predicted to be at 25°S–12°N in DJF, and at 13°S–28°N in JJA (Figure 3a). The upward velocities are predicted to be reduced where ascending branches are located (Figure 3b), except that the main equatorial convection zone (about 0–5°S in DJF and 2–8°N in JJA) is predicted to be stronger and penetrate higher in year 2100 than in year 2000, a result that again agrees qualitatively with that of *Dai et al.* [2001]. As a result, the precipitation associated with the main equatorial convection zone is enhanced, while that associated with the rest of the ascending branches of the Hadley cells is reduced (Figures 2c and 2d). The changes in the stream function relative to year 2000 (Figure 3c) also indicate the weakening of the Hadley and Ferrell cells. The predicted weakening in Hadley cells depends on the changes in latitudinal temperature gradient between the tropics and subtropics [*Rind and Rossow*, 1984]. In previous studies that have examined climate change with doubled CO_2, the Hadley Cells are predicted in some studies to be weakened [*Rind et al.*, 1990; *Dai et al.*, 2001; *Rind et al.*, 2001; *Holzer and Boer*, 2001] and in others to be enhanced [*Rind et al.*, 1998]. *Hansen et al.* [2005] also predicted that the changes in greenhouse gases from the preindustrial time to present-day have led to a strengthening of the Hadley Cells.

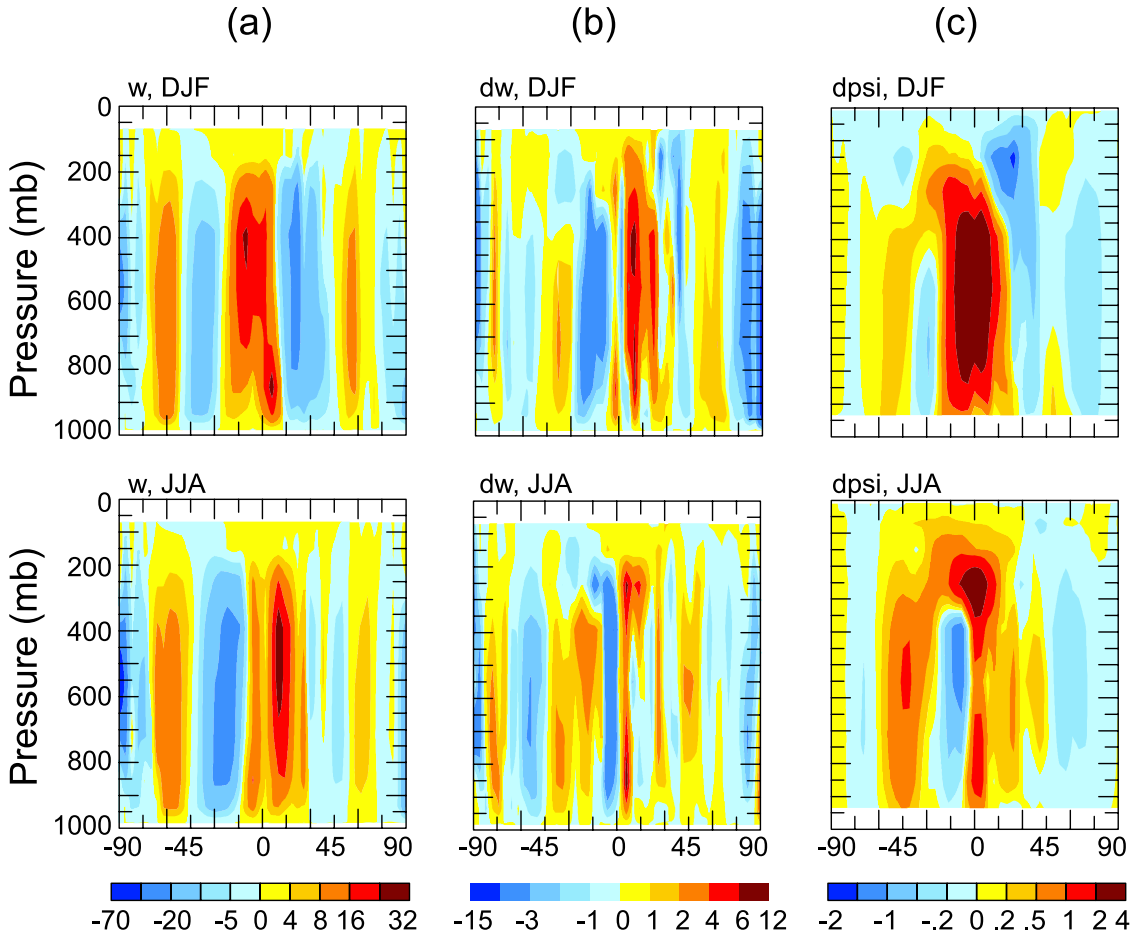

Figure 3. Latitude-pressure distributions of zonal and seasonal mean (a) present-day vertical velocity (10^{-5} mb s^{-1}), (b) changes in vertical velocity (10^{-5} mb s^{-1}) from year 2000 to year 2100, and (c) changes in mass stream function (10^{10} kg s^{-1}) from 2000 to 2100. Positive values of the mass stream function indicate anticlockwise circulation.

[28] Predicted changes in annual mean surface wind speed over 2000–2100 are shown in Figure 4a. Local changes in surface wind speed lie mostly within ±1.0 m s^{-1}, with changes exceeding 1.0 m s^{-1} predicted only over the northwestern and tropical Pacific Ocean. Zonal mean changes in surface wind speed (Figure 4b) are predicted to be within ±0.37 m s^{-1}. Zonal mean reductions in wind speed are predicted at 30–60°S, 5°S–40°N, and around 60°N.

4. Effects of CO_2-Driven Climate Change on Tropospheric Ozone and Aerosols

[29] To separate the effects of CO_2-driven (pure) climate change from those of changing non-CO_2 anthropogenic emissions, we hold non-CO_2 anthropogenic emissions at present-day levels with the allowance that climate-sensitive emissions respond to the climate change. We examine the changes in levels of O_3 and aerosols (CL2100EM2000 - CL2000EM2000) resulting from pure climate change in the absence of heterogeneous reactions. The effects of pure climate change in the presence of heterogeneous reactions do not differ qualitatively from those in their absence, except those discussed at the end of this section. Predicted changes in global burdens of ozone and aerosols as a result of pure climate change are summarized in Table 4.

4.1. Predicted Changes in Ozone

[30] Figure 5a shows the effect of CO_2-driven climate change on surface-layer ozone mixing ratios (CL2100EM2000 - CL2000EM2000) for January and July. Ozone concentrations are generally lower in the warmer climate, except for those near heavily populated and biomass burning areas. July O_3 mixing ratios over the eastern United States, Europe, and South Africa, as well as those near the east coast of China are predicted to increase by up to 8–12 ppbv. In January, ozone concentrations over biomass burning areas in Africa are predicted to increase by as much as 11 ppbv. The predicted regional increases of O_3 can be explained as follows. Global temperature increase leads to less vigorous atmospheric flow, resulting in near-source enhancement of tracer mixing ratios [*Boer*, 1995; *Carnell and Senior*, 1998; *Holzer and Boer*, 2001]. Increases in ozone also result from increases in emissions of biogenic hydrocarbons as surface temperature increases. As shown in Table 3, emissions of biogenic hydrocarbons are predicted to increase by 55% by year 2100. Sensitivity studies in the absence or presence of temperature depen-

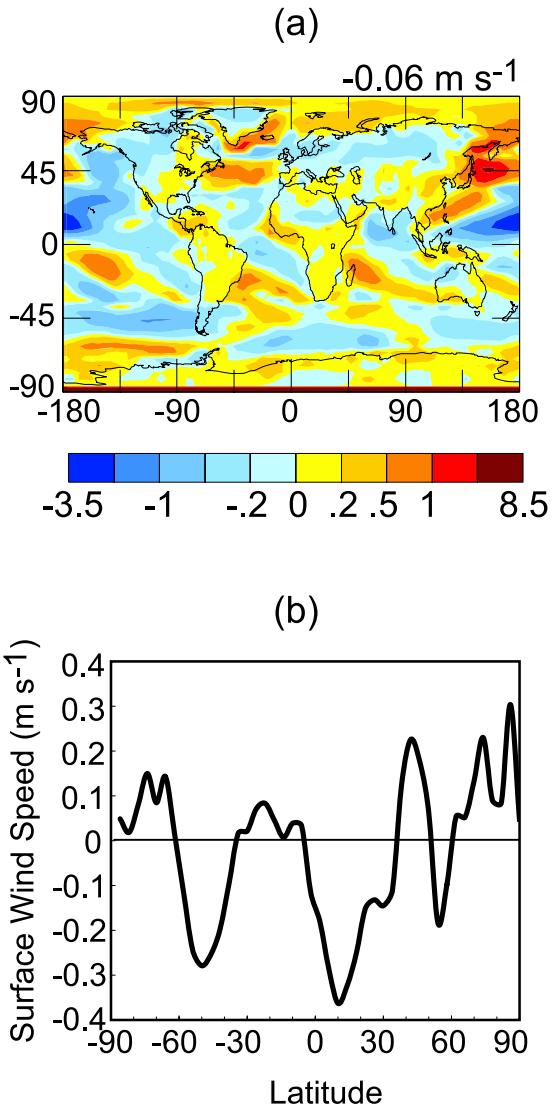

Figure 4. Predicted changes (m s^{-1}) in (a) annual mean surface wind speed and (b) zonal annual mean surface wind speed from 2000 to 2100. The global mean change is indicated for Figure 4a.

dence of biogenic emissions indicate that the increases in biogenic hydrocarbon emissions explain about 30–50% of the predicted increases in O_3 in the areas mentioned above. The climate-induced increases in biogenic hydrocarbons were also found to increase future daily maximum O_3 concentrations in summertime over the eastern United States [*Hogrefe et al.*, 2004]. Some other processes might also contribute to those regional increases of O_3. Peroxyacetyl nitrate (PAN) will be less stable at higher temperatures, so oxidized nitrogen is more likely to be present as NO_x near source regions [*Stevenson et al.*, 2005]. *Murazaki and Hess* [2006] found that the higher levels of water vapor have different effects on O_3, depending on the background NO_x level; with increased water vapor in a warmer climate, O_3 destruction is enhanced at low NO_x levels, while O_3 production is enhanced if NO_x concentrations are high.

[31] The zonal mean percentage changes in O_3 concentrations are shown in Figure 5b for January and July. Zonal mean O_3 concentrations are reduced throughout the troposphere as a result of CO_2-induced warming, with the largest percentage reductions of 20–30% predicted near the surface over the North Pole, over the tropics and subtropics in the lower troposphere, and within ±30° near the tropopause, correlating with the predicted largest increases in temperature or water vapor. Increased water vapor has an overall effect of leading to more ozone loss through ozone photolysis followed by $O^1(D)$ reaction with H_2O, which, together with the increase in temperature, leads to a reduction in net chemical production of O_3 [*Johnson et al.*, 2001]. Global O_3 budgets from CL2100EM2000 and CL2000EM2000 (Table 5) give a net chemical O_3 production of 412 Tg yr^{-1} under present-day climate conditions, and 331 Tg yr^{-1} in the year 2100 atmosphere. Pure CO_2-induced climate change is predicted to reduce the global ozone burden by 12%, from 349 Tg in present-day to 307 Tg with year 2100 climate.

4.2. Predicted Changes in Carbonaceous Aerosols

[32] Figure 6 shows the changes (CL2100EM2000 - CL2000EM2000) in BC, POA, and SOA concentrations resulting from the climate change alone at selected vertical levels. BC and POA aerosols are chemically inert tracers

Table 4. Predicted Annual Mean Global Burdens[a]

	No Heterogeneous Chemistry			
Species	CL2000EM2000	CL2100EM2000	CL2000EM2100	CL2100EM2100
O_3	349	307 (−12.0%)	602 (+72.5%)	521 (+49.3%)
H_2O_2	3.37	4.21 (+24.9%)	7.16 (+112.5%)	8.86 (+162.9%)
SO_2	1.14	0.96 (−15.8%)	0.59 (−48.2%)	0.57 (−50.0%)
SO_4^{2-}	2.14	1.84 (−14.0%)	1.96 (−8.4%)	1.79 (−16.4%)
NO_3^-	0.53	0.28 (−47.2%)	2.43 (+358.5%)	1.49 (+181.1%)
BC	0.23	0.20 (−13.0%)	0.54 (+134.8%)	0.48 (+108.7%)
POA	1.29	1.17 (−9.3%)	2.96 (+129.5%)	2.72 (+110.9%)
SOA	0.35	0.38 (+8.6%)	0.46 (+31.4%)	0.54 (+54.3%)
Sea salt	5.44	4.39 (−19.3%)	5.44 (0%)	4.39 (−19.3%)
Mineral dust	18.17	15.20 (−16.3%)	18.17 (0%)	15.20 (−16.3%)
	With Heterogeneous Chemistry			
Species	CL2000EM2000h	CL2100EM2000h	CL2000EM2100h	CL2100EM2100h
O_3	313	277 (−11.5%)	509 (+62.6%)	450 (+43.8%)
SO_4^{2-}	1.42	1.30 (−8.5%)	1.39 (−2.1%)	1.33 (−6.3%)
NO_3^-	0.51	0.27 (−47.1%)	2.02 (+296.1%)	1.27 (149.0%)

[a]Numbers in parentheses are percentage changes compared with present-day climate and emissions (CL2000EM2000 or CL2000EM2000h). Units are in Tg.

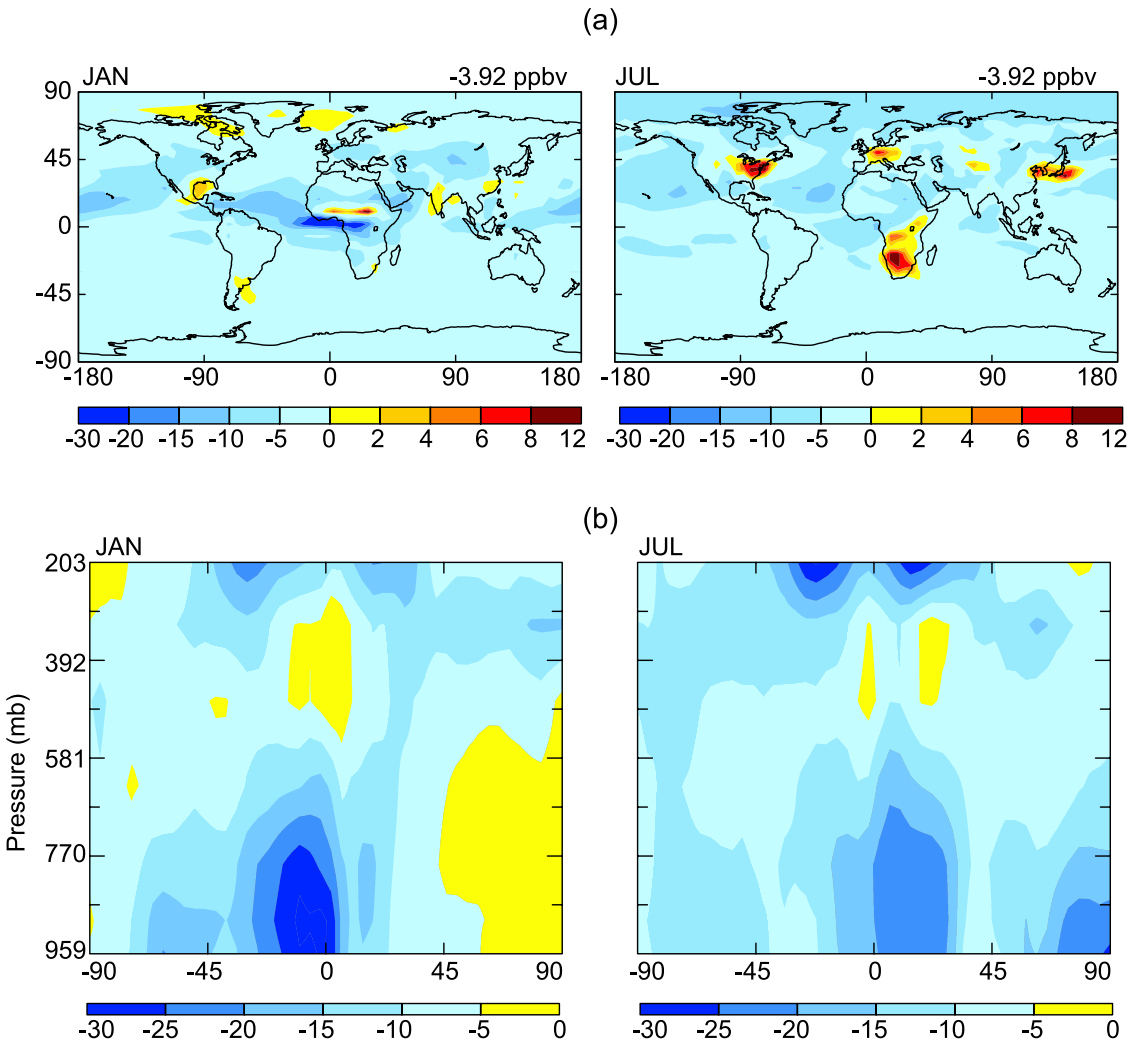

Figure 5. (a) Changes in January and July predicted surface-layer ozone concentrations (ppbv, CL2100EM2000-CL2000EM2000) resulting from CO_2-driven equilibrium climate change over 2000–2100. Global mean change is indicated at the top right corner of each panel. (b) Percentage changes ((CL2100EM2000-CL2000EM2000) × 100/CL2000EM2000) in January and July zonal mean ozone concentrations.

that respond to changes in meteorological fields. The pattern of the predicted changes in BC is similar to that of the changes in POA. POA concentrations in the tropics are predicted to increase. POA aerosols near the equator arise mainly from biomass burning sources located in South America and Africa, as well as biomass burning and fossil fuel emissions in South Asia. In a warmer climate, the weaker Hadley cell leads to weaker trade winds and consequently less POA being transported away from the source regions; this finding agrees with that reported by *Holzer and Boer* [2001]. The weaker Hadley cell leads to reduced precipitation (Figure 2) and weaker upward transport in tropics (Figure 3), which also helps to increase POA concentrations.

[33] Surface POA concentrations are predicted to generally decrease from mid to high latitudes in both hemispheres, as a result of increased precipitation (Figure 2c). The effects of climate change on POA concentrations over North America, Europe, and eastern China depend on the changes in precipitation and transport. While slower transport in the warmer climate increases POA concentrations near the source regions, larger annual mean precipitation in these populated areas leads to larger wet deposition of hydrophilic POA (50% of emitted POA is assumed to be hydrophilic [*Liao et al.*, 2003]). The net effect of these two competing factors leads to a complex response: increased POA concentrations over and near western Europe, and reduced concentrations over the United States and eastern China (Figure 6b). The predicted 10% increase in global mean precipitation in year 2100 has a large impact on aerosol loadings. The predicted annual global budget of POA shows that climate change alone leads to a reduction in POA global burden of 9.3%, from 1.29 Tg in present-day to 1.17 Tg in year 2100, as a result of a 3.8% increase (from 50.2 Tg yr^{-1} in present-day to 52.1 Tg yr^{-1} in year 2100) in POA wet deposition. The global BC burden is predicted to be reduced by 13% (Table 4) for the same reason.

[34] Climate change influences SOA distributions in several ways. First, increased precipitation leads to in-

Table 5. Global Budget for Tropospheric O_3[a]

	CL2000EM2000	CL2100EM2000	CL2000EM2100	CL2100EM2100
Sources, Tg O_3 yr^{-1}				
In situ chemical production	4384	4799	10076	10811
Transport from stratosphere	401	401	401	401
Total sources	4785	5200	10477	11212
Sinks, Tg O_3 yr^{-1}				
In situ chemical loss	3972	4468	8965	9832
Dry deposition	808	724	1541	1386
Total sinks	4780	5192	10479	11218
Burden, Tg O_3	349	307	602	521
Lifetime, days	27	22	21	17
Net chemical production	412	331	1111	979

[a]Budgets are for the odd oxygen family defined as the sum of O_3, O, NO_2, 2 × NO_3, HNO_4, 3 × N_2O_5, and the peroxyacyl nitrates. Values are averaged over the 5-year chemistry simulation.

creased wet deposition of SOA and its gas-phase precursors, as well as less POA available for the absorption of SOA. Also, higher temperatures shift the gas-particle partitioning of volatile oxidation products toward the gas-phase. Each of these effects leads to decreased SOA. On the other hand, there is a 58% predicted increase in emissions of monoterpenes and ORVOCs in year 2100 (Table 3). The net effect of these opposing influences is a modest increase in global

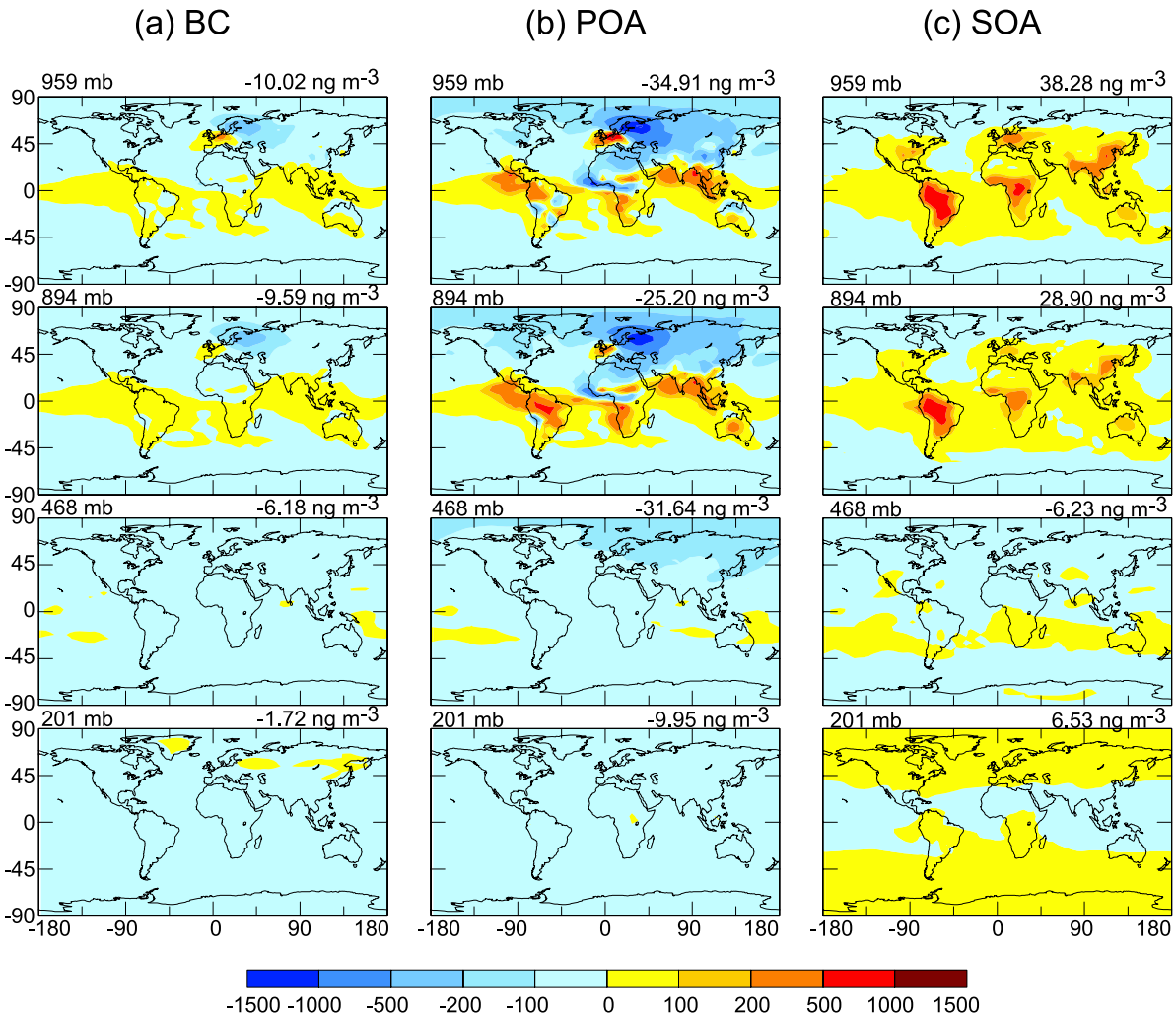

Figure 6. Changes in annual mean concentrations (ng m^{-3}, CL2100EM2000-CL2000EM2000) of (a) BC, (b) POA, and (c) SOA, at selected layers resulting from the CO_2-driven climate change over 2000–2100. Global mean change is indicated at the top right corner of each panel.

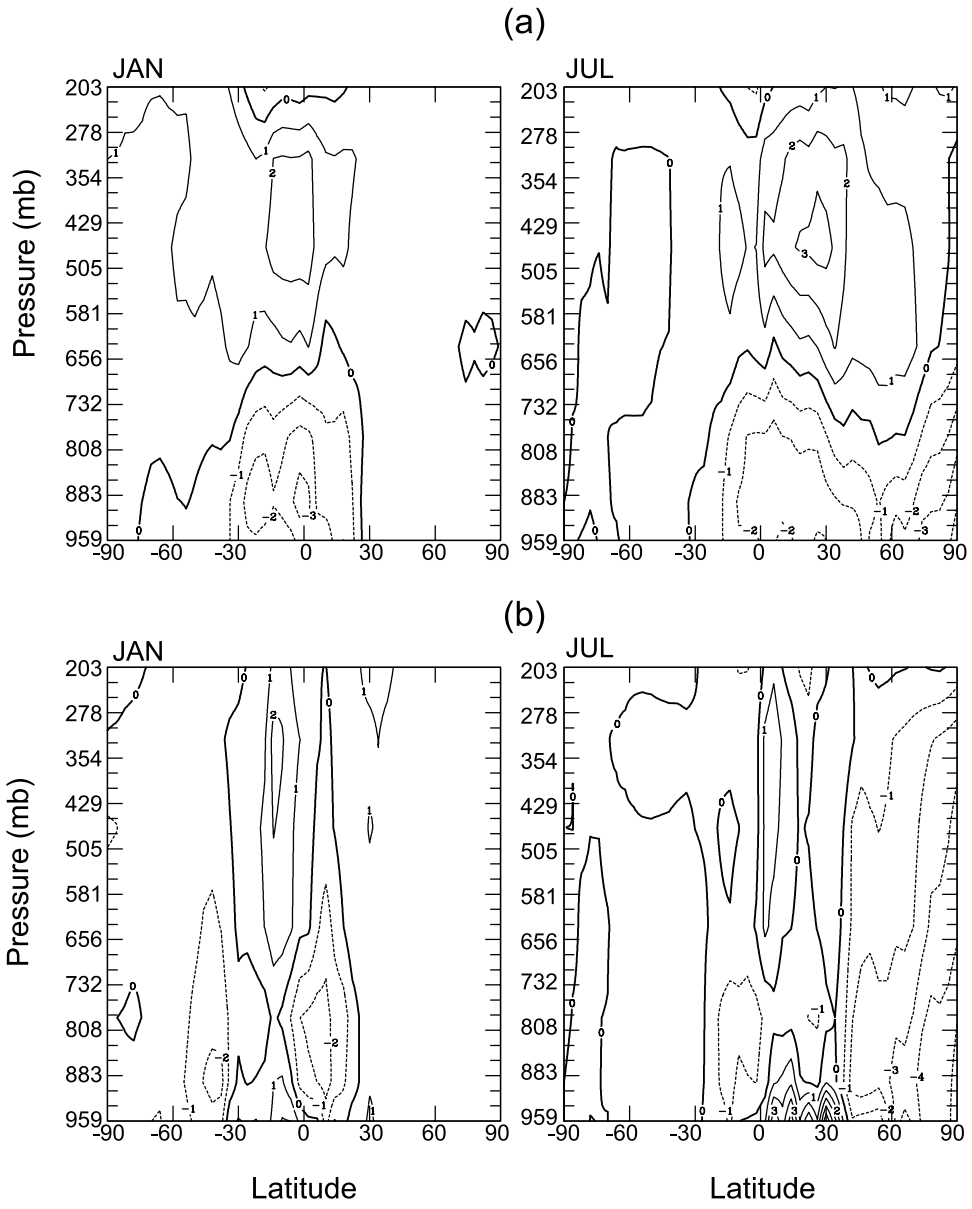

Figure 7. (a) Zonal mean changes in OH concentrations (10^5 radicals cm^{-3}) resulting from CO_2-driven climate change (CL2100EM2000 - CL2000EM2000). (b) Zonal mean changes in OH concentrations (10^5 radicals cm^{-3}) resulting from the changes in both climate and emissions (CL2100EM2100 - CL2000EM2000). Left panels are for January, and right panels are for July.

SOA from 2000 to 2100. With anthropogenic POA emissions held at present-day levels, the predicted SOA burden is 0.38 Tg in year 2100 atmosphere, an 8.6% increase relative to the 0.35 Tg predicted with the present-day climate (Table 4).

4.3. Predicted Changes in Sulfate and Nitrate Aerosols

[35] Dimethyl sulfide (DMS) emissions depend on ocean surface wind speed and temperature. In year 2100 climate, while higher temperature increases DMS emissions, the slower wind speed over the oceans (Figure 3b) reduces air-sea exchange. The temperature effect dominates, leading to an overall increase in DMS emissions by about 11% from 2000 to 2100 (Table 3). Note that this estimate is based on an assumption of constant marine DMS concentrations. *Bopp et al.* [2004] predicted a 3% increase in DMS emissions on the basis of the GCM predicted sea-surface DMS concentrations and a doubled CO_2 climate.

[36] Both the oxidation of DMS and sulfate formation from the gas-phase reaction of SO_2 + OH are determined by tropospheric OH concentrations. We show in Figure 7a the predicted zonal mean changes in OH concentration in the warmer climate (CL2100EM2000 - CL2000EM2000). In both January and July, OH concentrations increase mainly above 650 mb altitude in the tropics of the summer hemisphere, corresponding to the region with the largest increases in water vapor. Over the tropics and in the summer hemisphere, OH concentrations in the lower troposphere are predicted to decrease, as a result of lower O_3 and increased

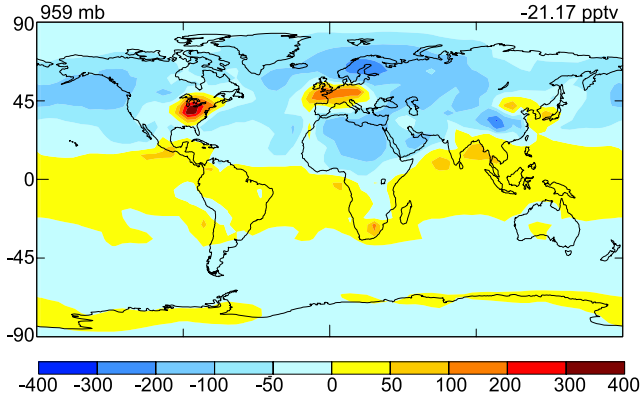

Figure 8. Predicted changes in annual mean sulfate concentration (pptv, CL2100EM2000-CL2000EM2000) at the surface layer resulting from CO_2-driven climate change from 2000 to 2100. Global mean change is indicated at the top right corner of the panel.

OH loss from the CH_4+OH reaction at higher temperature [*Johnson et al.*, 1999].

[37] The annual mean changes in surface layer sulfate mixing ratios (CL2100EM2000 - CL2000EM2000) by CO_2-induced warming are presented in Figure 8. The predicted changes in surface-layer sulfate mixing ratios are similar to those of POA, with sulfate mixing ratios reduced at the middle to high latitudes in both hemispheres but increased over the tropics. The surface-layer sulfate mixing ratios over Europe, the eastern United States, and eastern China are predicted to increase by up to 400 pptv. Besides the near-source effects mentioned in connection with POA, the locally higher O_3, OH, and H_2O_2 concentrations in the warmer climate contribute to larger sulfate formation in these areas. Although the zonal mean surface-layer OH concentrations decrease, the predicted OH concentrations near sources increase corresponding to the locally increased O_3 (Figure 5). H_2O_2 formation increases in a warmer climate, because the rate coefficient of the reaction $HO_2 + HO_2 \rightarrow H_2O_2$ increases with temperature. The global burden of H_2O_2 is predicted to increase by 25% as a result of climate change alone (Table 4).

[38] The global annual sulfate budget is given in Table 6. Climate change alone slightly reduces sulfate formation via the gas-phase OH reaction while increasing in-cloud formation by about 5%. Sulfate lifetime is reduced from 4.7 days to 4.0 days as a result of the increased wet deposition. The global burdens of SO_2 and sulfate are predicted to be reduced by 16% and 14%, respectively, in the warmer climate (Table 4).

[39] Changes in temperature influence aerosol equilibrium significantly. Figure 9 shows the ratios of the predicted zonal mean nitrate concentrations from the simulation CL2100EM2000 to those from CL2000EM2000. In the warmer climate, more HNO_3 remains in the gas-phase, leading to significant percentage reductions in nitrate concentrations throughout the troposphere except in the tropical lower troposphere. The reasons for the increases over the tropics are the same as those for the increases of POA in that region. The global burden of nitrate is predicted to be reduced by 47.2% as a result of CO_2 warming over 2000–2100, if emissions of nitrate precursors remain at 2000 levels.

4.4. Predicted Changes in Sea Salt and Mineral Dust

[40] As shown in Table 3, sea salt emissions are predicted to be reduced by 6% as a result of the reductions in zonal mean surface wind speed at 30–60°S, 5°S–40°N, and around 60°N (Figure 4b). These reductions in emissions, together with the increases in precipitation, lead to a predicted overall 19% reduction in global sea salt burden from the present-day to year 2100 (Table 4).

[41] Mineral dust emissions depend on both wind speed and soil moisture. With the predicted reductions in surface wind speed over the Sahara Desert and central Asia (Figure 4a), two major sources of mineral dust, and the increases in precipitation over North Africa, a 14% reduction in dust emissions from year 2000 to year 2100 is predicted (Table 3). Since the increased precipitation also leads to larger wet deposition of dust, the predicted global burden of dust is reduced from 18.2 Tg in present-day to 15.2 Tg in year 2100 (Table 4). Because land type and vegetation are likely to change as climate changes, more accurate simulation of future mineral dust requires prognostic simulation of land surface use.

[42] The changes in emissions of sea salt and mineral dust predicted in this work diverge from those in Chapter 5.5.2 of the IPCC 2001 report. The IPCC estimates were based on the ratios of monthly average wind speeds for the years 2090–2100 to those for the years 1990–2000 associated with the IS92a scenario simulated by *Dai et al.* [2001].

Table 6. Global Budget for Sulfate Aerosol

	CL2000EM2000	CL2100EM2000	CL2100EM2100
Sources, Tg S yr^{-1}			
Industrial emissions	2.07	2.07	1.81
SO_2 + OH	11.35	11.13	11.42
In-cloud SO_2 + H_2O_2	32.91	35.75	41.47
In-cloud SO_2 + O_3	9.49	8.63	5.22
Total sources	55.82	57.58	59.92
Sinks, Tg S yr^{-1}			
Dry deposition	8.70	8.06	8.27
Wet deposition	45.93	48.29	49.62
Total sinks	54.63	56.35	57.89
Burden, Tg S	0.71	0.61	0.60
Lifetime, days	4.7	4.0	3.8

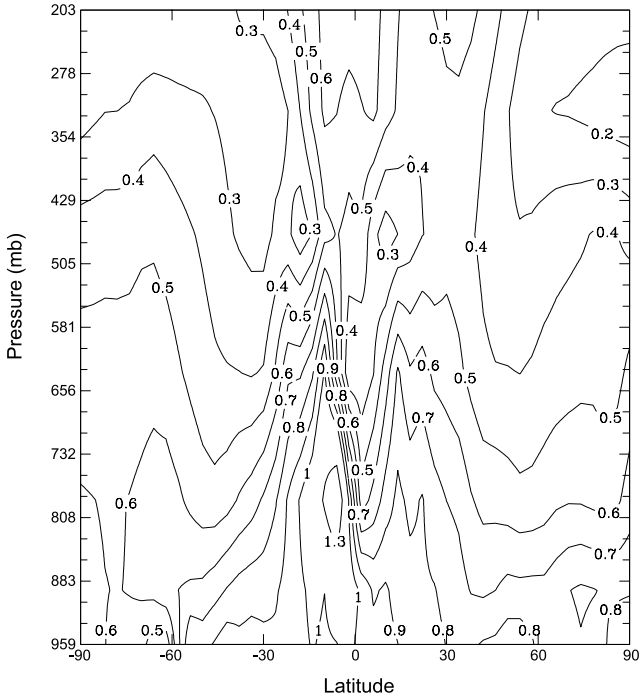

Figure 9. Ratios of the predicted annual and zonal mean nitrate concentrations from CL2100EM2000 to those from CL2000EM2000.

Although the changes in temperature, precipitation, and meridional circulations predicted here agree qualitatively with those of *Dai et al.* [2001], our equilibrium climate simulation with IPCC SRES A2 CO_2 only is different from the transient climate simulation with IS92a sulfate, CO_2, and non-CO_2 greenhouse gases by *Dai et al.* [2001]. As discussed by *Dai et al.* [2001], the predicted regional climate changes may also be model dependent.

4.5. Effects of Climate Change in the Presence of Heterogeneous Reactions

[43] The heterogeneous reactions considered are those of N_2O_5, NO_3, NO_2, and HO_2 on wet aerosols, the uptake of SO_2 by sea salt, as well as the uptake of SO_2, HNO_3 and O_3 by mineral dust; the heterogeneous reactions influence mainly the concentrations of O_3, sulfate, and nitrate [*Liao and Seinfeld*, 2005]. The effects of climate change on the predictions of O_3, sulfate, and nitrate in the presence of the heterogeneous reactions are represented by the differences in concentrations between the simulations CL2100EM2000h and CL2000EM2000h. The annual mean differences between the effects of climate change with heterogeneous reactions and those without [(CL2100EM2000h - CL2000EM2000h) - (CL2100EM2000 - CL2000EM2000)] are shown in Figure 10 for the surface layer.

[44] The effects of climate change on surface O_3 concentrations in the presence of heterogeneous reactions are qualitatively the same as those shown in Figure 5 in their absence. However, since the uptake coefficient for the hydrolysis of N_2O_5 depends on temperature and relative humidity [*Evans and Jacob*, 2005; *Liao and Seinfeld*, 2005], at higher atmospheric temperature, hydrolysis of N_2O_5 is reduced [*Hallquist et al.*, 2003], leading to more NO_x and hence larger increases in O_3 concentrations near sources and less O_3 reduction in other areas, as indicated by the positive values shown in Figure 10a. On an annual mean basis, the climate-induced changes in surface O_3 concentrations predicted in the presence of heterogeneous reactions differ from those predicted in their absence by 1–4 ppbv in the Northern Hemisphere where aerosol concentrations are high.

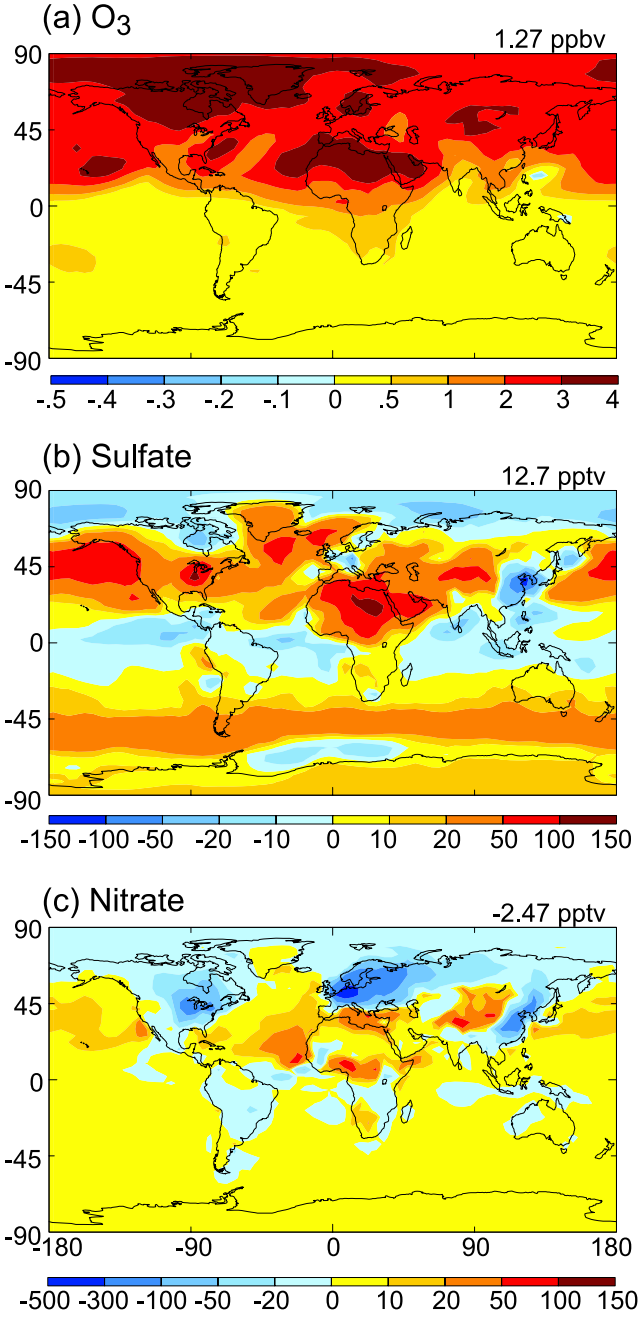

Figure 10. Annual mean differences between the effects of CO_2-driven climate change in the presence and absence of heterogeneous reactions [(CL2100EM2000h - CL2000EM2000h) - (CL2100EM2000 - CL2000EM2000)] for the surface-layer concentrations of (a) O_3, (b) sulfate, and (c) nitrate. The global mean value is indicated at the top right corner of each panel.

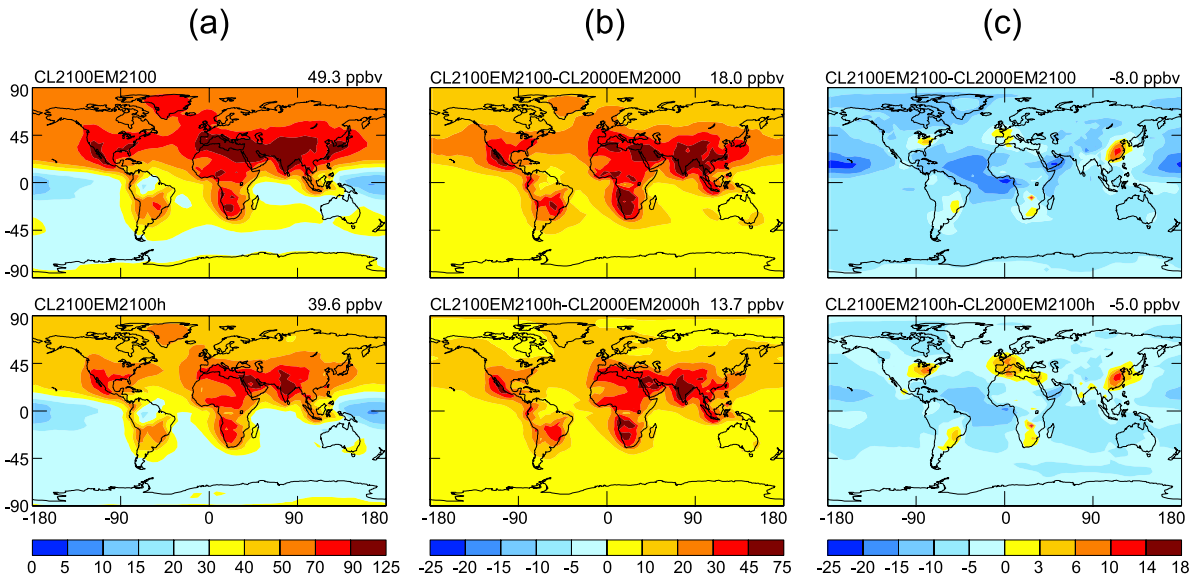

Figure 11. (a) Predicted year 2100 surface-layer O_3 mixing ratios (ppbv) with changes in both climate and emissions. (b) Predicted changes in surface-layer O_3 mixing ratio (ppbv) from 2000 to 2100. (c) Differences (ppbv) between surface-layer O_3 mixing ratios simulated with changes in both climate and emissions and those with changes in emissions only. Top panels are simulated in the absence of the heterogeneous reactions as discussed in the text, while the bottom panels include heterogeneous reactions. The global mean value is indicated at the top right corner of each panel.

[45] In the absence of sea salt and mineral dust uptake of SO_2, the surface-layer sulfate concentrations are predicted to be reduced at middle to high latitudes in both hemispheres (Figure 8). Because of the predicted reductions in sea salt and mineral dust burdens in year 2100, less SO_2 is taken up by sea salt and dust. As a result, the largest differences in the effects of pure climate change on sulfate are predicted over oceans and near dust sources (Figure 10b).

[46] Predicted climate-induced reductions in surface-layer nitrate concentrations in the presence of heterogeneous reactions are less over the oceans and near the dust sources, again because of the reduced uptake of HNO_3 by sea salt and mineral dust in year 2100 (Figure 10c). Over Europe, eastern Asia, and the eastern United States, climate-induced reductions of nitrate concentrations in the presence of heterogeneous reactions exceed those in their absence, as a result of the less hydrolysis of N_2O_5 at higher temperature and hence less HNO_3 available for nitrate formation in year 2100.

[47] It should be noted that the results shown in Figure 10 are based on the changes in climate alone. Heterogeneous reactions assume greater importance when year 2100 anthropogenic emissions are used in the chemistry simulations. With the large increases in aerosol concentrations and NO_x emissions in year 2100, hydrolysis of N_2O_5 becomes more influential in predicting O_3 and nitrate formation [*Liao and Seinfeld*, 2005].

5. Predicted O_3 and Aerosol Concentrations With Year 2100 Projected Emissions and Climate

[48] Predicted year 2100 surface-layer O_3 mixing ratios, the changes relative to the year 2000 concentrations, and the differences between the surface-layer O_3 mixing ratios simulated with the changes in both climate and emissions and those obtained with changes in emissions only are shown in Figure 11. Compared to the present-day O_3 levels, year 2100 surface-layer O_3 concentrations are predicted to generally increase by 30–70 ppbv over populated and biomass burning areas (Figure 11b). Such large increases in O_3 concentrations over the emission source regions result mainly from the increases in anthropogenic emissions of O_3 precursors over 2000–2100, but climate change also contributes to the increases. As shown in Figure 11c, accounting for the changes in emissions and climate, the surface-layer O_3 concentrations over or near emission source areas increase by up to 17 ppbv, relative to the case in which only emission changes are considered. Climate change alone has the overall effect of reducing global O_3 burden; the year 2100 global O_3 burden of 521 Tg (or 450 Tg) predicted in CL2100EM2100 (or CL2100EM2100h) is about 13.4% (or 11.6%) lower than that predicted in CL2000EM2100 (or CL2000EM2100h) (Table 4). The difference in predicted O_3 burden between CL2100EM2100h and CL2100EM2100 reflects the importance of heterogeneous reactions.

[49] With changes in emissions and climate considered, burdens of all anthropogenic aerosol species increase from 2000 to 2100 except for sulfate (Table 4). Relative to year 2000, the predicted sulfate burden is lower in year 2100, as a result of the projected lower emissions and larger wet deposition (Table 6). While sulfate is the most significant anthropogenic aerosol component in 2000, POA is predicted to have the largest global burden in 2100, followed by sulfate, nitrate, and BC. Although the warmer climate does not favor the formation of nitrate aerosol, the nitrate burden is predicted to increase from 0.53 Tg (or 0.51 Tg) in 2000 to 1.49 Tg (or 1.27 Tg) in 2100 in the absence (or presence) of heterogeneous reactions, as a result of the significant increases in NO_x and NH_3 emissions.

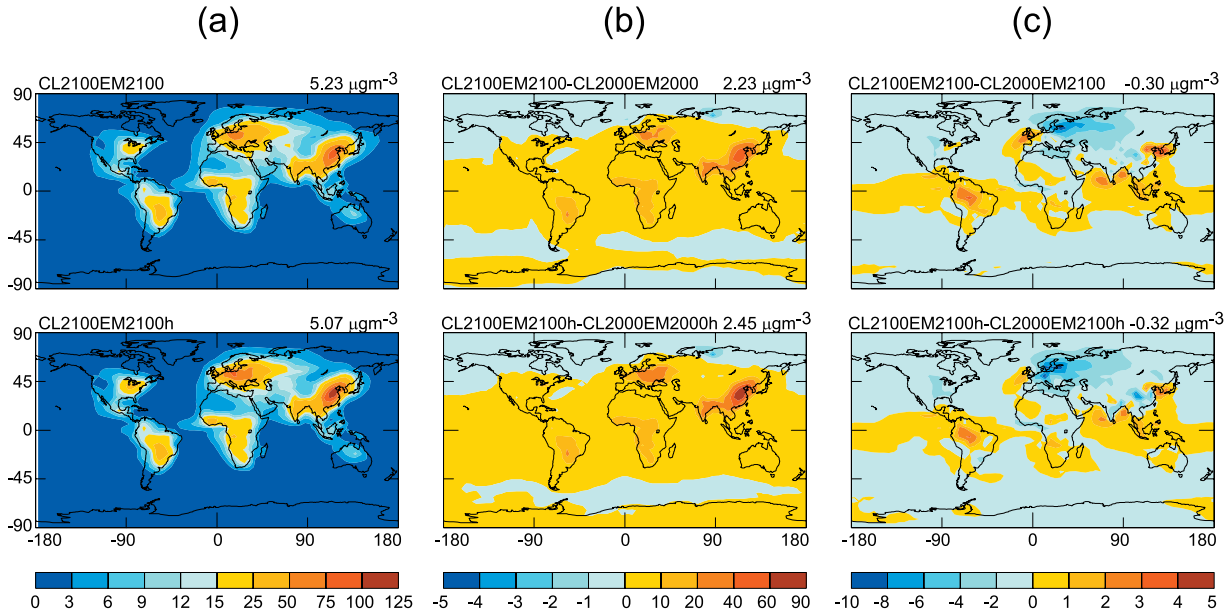

Figure 12. (a) Predicted year 2100 surface-layer dry aerosol mass concentrations (μg m^{-3}) with changes in both climate and emissions. Dry aerosol mass is the sum of sulfate, nitrate, ammonium, BC, POA, and SOA. (b) Predicted changes in surface-layer dry aerosol mass concentrations (μg m^{-3}) from 2000 to 2100. (c) Differences (μg m^{-3}) between surface-layer dry aerosol mass concentrations simulated with changes in both climate and emissions and those with changes in emissions only. Top panels are simulated in the absence of the heterogeneous reactions as discussed in the text, while the bottom panels include heterogeneous reactions. The global mean value is indicated at the top right corner of each panel.

[50] Figure 12a shows the year 2100 dry aerosol mass, the sum of sulfate, nitrate, ammonium, BC, POA, and SOA, at the surface layer from the simulations CL2100EM2100 and CL2100EM2100h. Dry aerosol mass concentrations exceeding 15 μg m^{-3} are predicted over Europe, the eastern United States, eastern China, and the biomass burning regions. As a result of the large increases in POA and nitrate, the dry mass concentrations over the eastern United States, Europe, and eastern Asia are predicted to increase by 0–10, 20–40, and 40–90 μg m^{-3}, respectively, relative to the present-day values (Figure 12b). The dry aerosol mass concentrations predicted in CL2100EM2100 (or CL2100EM2100h) differ from those predicted in CL2000EM2100 (or CL2000EM2100h) by −10 μg m^{-3} to +4 μg m^{-3} regionally (Figure 12c).

[51] The global budgets for year 2100 O_3 and sulfate in the absence of heterogeneous reactions are given in Tables 5 and 6, respectively. When changes in emissions and climate are accounted for, the lifetime of O_3 changes from 27 days in present-day to 17 days in year 2100, while that of sulfate changes from 4.7 to 3.8 days. In year 2100, the shorter lifetime of O_3 is caused mainly by the increased removal of O_3 by the reaction of $O^1(D)$ with H_2O [*Johnson et al.*, 1999, 2001], while the shorter lifetime of sulfate results from increased wet removal.

6. Impact of Climate Change on Estimates of Year 2100 Direct Radiative Forcing

[52] To examine the effect of climate change on future forcing estimates, we compare the instantaneous radiative forcings calculated using CL2000EM2100 concentrations and climate with those calculated with CL2100EM2100 conditions. Radiative forcings by O_3, sulfate, nitrate, BC, OC (POA+SOA), as well as by the internal and external mixtures of these aerosols are calculated. In the external mixture, particles from different sources remain separated, while in the internal mixture, the various chemical components are mixed uniformly in each particle. The top of the atmosphere (TOA) forcing by a species is calculated as the difference in the net fluxes at TOA in its presence and absence, so the forcing values reported here represent the effect of both natural and anthropogenic ozone/aerosols on global radiative balance. The assumptions for water uptake by aerosols, aerosol size distributions, and refractive indices follow those described by *Liao et al.* [2004].

[53] The global and annual mean TOA O_3 and aerosol forcings from simulations CL2000EM2100, CL2100EM2100, CL2000EM2100h, and CL2100EM2100h are summarized in Table 7. Compared with the TOA O_3 forcing calculated in simulation CL2000EM2100, the 13% lower global O_3 burden and the different climate in simulation CL2100EM2100 lead to 20% reduction in global mean O_3 radiative forcing (Tables 5 and 7). In the warmer climate, the reduced burden and the melting of snow and ice lead to 0.2–0.4 W m^{-2} reductions in shortwave O_3 forcing at the North Pole, and the reduced O_3 burden also leads to about the same magnitude reductions in O_3 longwave forcing over tropics and subtropics.

[54] Although the global BC burden predicted in CL2100EM2100 is just 11% lower than that predicted in CL2000EM2100, the global mean BC forcing is reduced by 23% in year 2100 climate (CL2100EM2100), because BC

Table 7. Year 2100 TOA Radiative Forcing[a]

	No Heterogeneous Reactions	
Species	CL2000EM2100	CL2100EM2100
O_3	0.42(S) + 0.64(L) = 1.06	0.33(S) + 0.52(L) = 0.85
Sulfate	−0.97	−0.93
Nitrate	−1.09	−0.78
BC	+1.26	+0.97
OC	−0.56	−0.58
INT	−0.26	−0.48
EXT	−1.22	−1.20
O_3 + INT	+0.80	+0.37
O_3 + EXT	−0.16	−0.35
	With Heterogeneous Reactions	
Species	CL2000EM2100h	CL2100EM2100h
O_3	0.36(S) + 0.57(L) = 0.93	0.29(S) + 0.47(L) = 0.76
Sulfate	−0.72	−0.72
Nitrate	−1.00	−0.74
BC	+1.26	+0.97
OC	−0.56	−0.58
INT	+0.06	−0.26
EXT	−0.87	−0.96
O_3 + INT	+0.99	+0.50
O_3 + EXT	+0.06	−0.20

[a]Units are W m^{-2}. Both natural and anthropogenic aerosols are considered in the forcing calculations. S, shortwave forcing by O_3; L, longwave forcing by O_3; INT, internally mixed sulfate, nitrate, BC, and OC (POA + SOA); EXT, externally mixed sulfate, nitrate, BC, and OC (POA + SOA).

forcing at high northern latitudes is reduced significantly as a result of the reduction in both BC column burden and surface albedo in the warmer climate. The global burden of OC predicted in CL2100EM2100 is 6% lower than that predicted in CL2000EM2100, but the global mean TOA forcing by OC changes slightly from −0.56 W m^{-2} in present-day climate to −0.58 W m^{-2} in the warmer climate. The TOA OC forcings over the polar regions change from warming in simulation CL2000EM2100 to cooling in simulation CL2100EM2100, because of the weak absorbing feature of OC and the reduced surface albedo in the warmer climate.

[55] Relative to simulation CL2000EM2100, the global mean sulfate cooling is 4% less with a 9% reduction in global burden in CL2100EM2100, and the global mean nitrate cooling is 28% less with a 39% reduction in global burden when climate change is considered (Tables 4 and 7). The percentage change in the global mean TOA forcing by a scattering aerosol is less than the percentage change in its global burden, because of the changes in surface albedo and clouds over polar regions and the predicted increases in concentrations in the tropics. Relative to simulation CL2000EM2100, sulfate TOA cooling in CL2100EM2100 increases at high northern latitudes, although sulfate column burdens there are predicted to be reduced. This forcing behavior at high latitudes is a result of reduced ice and snow cover, as well as fewer low clouds and more high clouds in the warmer climate. As shown by *Liao and Seinfeld* [1998], TOA sulfate cooling under clear sky conditions increases when surface albedo decreases, and thin stratus or cirrus clouds above sulfate aerosol enhance sulfate cooling.

[56] Global mean TOA forcing by the internal mixture of sulfate, nitrate, BC, and OC changes from −0.26 W m^{-2} in CL2000EM2100 to −0.48 W m^{-2} in CL2100EM2100, while the global mean forcing by the external mixture in year 2100 climate differs from that in year 2000 climate by the modest amount of 0.02 W m^{-2} (Table 7). Because an internal mixture has lower single-scattering albedo and hence stronger absorption of both incoming and outgoing solar radiation than an external mixture, the radiative forcing by an internal mixture is more sensitive to the changes in surface albedo. At the high northern latitudes, TOA forcing by either the internal or the external mixture is always positive, but the heating estimated in CL2100EM2100 is 2–4 W m^{-2} (or 1–2 W m^{-2}) less than that calculated in CL2000EM2100 for the internal (or external) mixture as a result of the reduction in surface albedo. Over populated areas, estimated TOA cooling by either the internal or the external mixture is 1–3 W m^{-2} less in year 2100 climate than in year 2000 atmosphere because of the reduction in aerosol column burdens.

[57] The effects of climate change on forcing estimates in the presence of heterogeneous reactions are similar to those predicted in their absence (Table 7); the CO_2-driven climate change is influential in estimating year 2100 TOA forcing of absorbing species and nitrate.

7. Summary and Discussion

[58] We have examined the impact of an equilibrium climate in year 2100 driven by the projected change in CO_2 concentration from IPCC SRES A2 on predictions of global ozone and aerosols by online GCM simulation of coupled tropospheric ozone-NO_x-hydrocarbon chemistry and sulfate, nitrate, ammonium, black carbon, primary organic carbon, secondary organic carbon, sea salt, and mineral dust aerosols.

[59] Using the GISS GCM II′ with a q-flux ocean, we predict an increase of 4.8°C in global mean surface air temperature in year 2100, as a result of the projected increase in CO_2 from 368 ppmv in year 2000 to 836 ppmv in year 2100. Year 2100 global mean precipitation is predicted to be 10% higher than that for year 2000; predicted changes in temperature and precipitation agree qualitatively with those of previous studies. The model predicts a weakening of the Hadley cells in the warmer 2100.

[60] We have performed four chemistry simulations, denoted CL2000EM2000, CL2100EM2000, CL2000EM2100, and CL2100EM2100, to assess the roles of CO_2-driven climate change and IPCC projected changes in emissions in influencing levels of tropospheric O_3 and aerosols. The differences between simulations CL2100EM2000 and CL2000EM2000 indicate that, with no changes in anthropogenic emissions, the CO_2-driven climate would change global O_3, sulfate, nitrate, BC, POA and SOA burdens by −12%, −14%, −47%, −13%, −9% and +9%, respectively. Although the global O_3 burden is predicted to be reduced as a result of faster removal of O_3 in the warmer climate, surface-layer O_3 concentrations over populated and biomass burning areas are predicted to increase as a result of climate change, owing to slower transport [*Holzer and Boer*, 2001], enhanced biogenic hydrocarbon emissions, decomposition of PAN at higher temperature, and the increase of O_3 production by increased water vapor at high NO_x levels. Climate

change influences aerosol burdens mainly by altering wet deposition, climate-sensitive emissions, and aerosol thermodynamic equilibrium.

[61] Accounting for both the CO_2-driven climate change and changes in emissions in simulation CL2100EM2100, the year 2100 global burdens of O_3, sulfate, nitrate, BC, POA and SOA are predicted to change by +49%, −16%, +181%, +109%,+111% and +54%, respectively, as compared with simulation CL2000EM2000. On the basis of the IPCC SRES A2 scenario, the changes in anthropogenic emissions play a more dominant role in determining future levels of tropospheric ozone and aerosols than does climate change. Sea salt and mineral dust burdens are predicted to be reduced by 19% and 16%, respectively, in the year 2100.

[62] We also examine the effects of CO_2-driven climate change on estimates of year 2100 direct radiative forcing by O_3 and aerosols. By comparing simulations CL2000EM2100 and CL2100EM2100, the effect of climate change alone on radiative forcings can be discerned; accounting for ozone and aerosols from both natural and anthropogenic sources, the predicted global mean TOA direct radiative forcings of O_3, sulfate, nitrate, BC, OC, internal mixture (internally mixed sulfate, nitrate, BC, and OC), and external mixture (externally mixed same aerosols) change from +1.06, −0.97, −1.09, +1.26, −0.56, −0.26, −1.22 W m^{-2} in CL2000EM2100 to +0.85, −0.93, −0.78, +0.97, −0.58, −0.48, −1.20 W m^{-2} in CL2100EM2100, respectively. The CO_2-induced changes in global burdens, surface albedo, and clouds have a large influence on radiative forcing of absorbing species and nitrate aerosol.

[63] The climate induced percentage changes in global O_3 and aerosol burdens as well as the absolute changes in year 2100 direct radiative forcings summarized above for the simulations in the absence of heterogeneous reactions agree closely with those obtained in their presence. When the reactions of N_2O_5, NO_3, NO_2, and HO_2 on wet aerosols, the uptake of SO_2 by sea salt, and the uptake of SO_2, HNO_3 and O_3 by mineral dust are considered, although hydrolysis of N_2O_5 is less in the warmer climate and the uptake by sea salt and mineral dust is reduced as a result of lower burdens of sea salt and mineral dust in year 2100, heterogeneous reactions are still influential in simulating year 2100 concentrations of O_3, sulfate, and nitrate; accounting for the changes in both climate and emissions, the year 2100 burdens of O_3, sulfate, and nitrate predicted in the presence of heterogeneous reactions are 14%, 26%, 15%, respectively, lower than those predicted in their absence.

[64] The results of this study suggest several avenues for improvement and future research. First, biogenic emissions of O_3 and SOA precursors as well as the mineral dust emissions are based on fixed vegetation and land types, which can be improved with a prognostic treatment of vegetation and land type. As shown by *Sanderson et al.* [2003] and *Lathière et al.* [2005], climate-vegetation coupling is important for predicting future biogenic hydrocarbon emissions. Second, O_3 transport from the stratosphere is fixed in all the simulations reported here; this process is climate-sensitive [*Sudo et al.*, 2003; *Collins et al.*, 2003; *Zeng and Pyle*, 2003] and can be improved with a GCM having a better representation of the stratosphere. Finally, and most importantly, the radiative effects of predicted ozone and aerosols in future years should be fed back into the GCM to assess complete chemistry-aerosol-climate coupling.

[65] **Acknowledgments.** This work was supported by the National Aeronautics and Space Administration Earth Observing System Interdisciplinary Science program (NASA EOS-IDS) and the U.S. Environmental Protection Agency under Science to Achieve Results (STAR) grant R830959. We also acknowledge the Center for Advanced Computing Research at Caltech for computing resources.

References

Adams, P. J., J. H. Seinfeld, D. M. Koch, L. Mickley, and D. Jacob (2001), General circulation model assessment of direct radiative forcing by the sulfate-nitrate-ammonium-water inorganic aerosol system, *J. Geophys. Res.*, *106*, 1097–1112.

Atherton, C. S., J. E. Penner, C. Price, and J. Walton (1995), Climate change and its effect on tropospheric ozone, in *Atmospheric Ozone as a Climate Gas, NATO ASI Ser., Ser. I*, vol. 32, edited by W.-C. Wang and I. S. A. Isaksen, pp. 65–85, Springer, New York.

Boer, G. J. (1995), Some dynamical consequences of greenhouse gas warming, *Atmos. Ocean*, *33*, 731–751.

Bopp, L., O. Boucher, O. Aumont, S. Belviso, J.-L. Dufresne, M. Pham, and P. Monfray (2004), Will marine dimethylsulfide emissions amplify or alleviate global warming?: A model study, *Can. J. Fish. Aquat. Sci.*, *61*, 826–835.

Bouwman, A. F., D. S. Lee, W. A. H. Asman, F. J. Dentener, K. W. Van Der Hoek, and J. G. J. Olivier (1997), A global high-resolution emission inventory for ammonia, *Global Biogeochem. Cycles*, *11*(4), 561–588.

Brasseur, G. P., J. T. Kiehl, J.-F. Mueller, T. Schneider, C. Granier, X. X. Tie, and D. Hauglustaine (1998), Past and future changes in global tropospheric ozone: Impact on radiative forcing, *Geophys. Res. Lett.*, *25*, 3807–3810.

Carnell, R. E., and C. A. Senior (1998), Changes in midlatitude variability due to increasing greenhouse gases and sulphate aerosols, *Climate Dyn.*, *14*, 369–383.

Chung, S. H., and J. H. Seinfeld (2002), Global distribution and climate forcing of carbonaceous aerosols, *J. Geophys. Res.*, *107*(D19), 4407, doi:10.1029/2001JD001397.

Collins, W. J., R. G. Derwent, B. Garnier, C. E. Johnson, M. G. Sanderson, and D. S. Stevenson (2003), Effect of stratosphere-troposphere exchange on the future tropospheric ozone trend, *J. Geophys. Res.*, *108*(D12), 8528, doi:10.1029/2002JD002617.

Constable, J. H., A. B. Guenther, D. S. Schimel, and R. K. Monson (1999), Modeling changes in VOC emission in response to climate change in the continental United States, *Global Change Biol.*, *5*, 791–806.

Dai, A., T. M. L. Wigley, B. A. Boville, J. T. Kiehl, and L. E. Buja (2001), Climates of the twentieth and twenty-first centuries simulated by the NCAR climate system model, *J. Clim.*, *14*(4), 485–519.

Evans, M. J., and D. J. Jacob (2005), Impact of new laboratory studies of N_2O_5 hydrolysis on global model budgets of tropospheric nitrogen oxides, ozone, and OH, *Geophys. Res. Lett.*, *32*, L09813, doi:10.1029/2005GL022469.

Gauss, M., et al. (2003), Radiative forcing in the 21st century due to ozone changes in the troposphere and the lower stratosphere, *J. Geophys. Res.*, *108*(D9), 4292, doi:10.1029/2002JD002624.

Gillette, D. (1978), A wind tunnel simulation of the erosion of soil: Effect of soil texture, sandblasting, wind speed, and soil consolidation on dust production, *Atmos. Environ.*, *12*, 1735–1743.

Griffin, R. J., D. R. Cocker, J. H. Seinfeld, and D. Dabdub (1999a), Estimate of global atmospheric organic aerosol from oxidation of biogenic hydrocarbons, *Geophys. Res. Lett.*, *26*, 2721–2724.

Griffin, R. J., D. R. Cocker, R. C. Flagan, and J. H. Seinfeld (1999b), Organic aerosol formation from the oxidation of biogenic hydrocarbons, *J. Geophys. Res.*, *104*, 3555–3567.

Guenther, A., et al. (1995), A global model of natural volatile organic compound emissions, *J. Geophys. Res.*, *100*, 8873–8892.

Hallquist, M., D. J. Stewart, S. K. Stephenson, and R. A. Cox (2003), Hydrolysis of N_2O_5 on sub-micron sulfate aerosols, *Phys. Chem. Chem. Phys.*, *5*(16), 3453–3463.

Hansen, J., A. Lacis, G. Russell, P. Stone, I. Fung, R. Ruedy, and J. Lerner (1984), Climate sensitivity: Analysis of feedback mechanisms, in *Climate Processes and Climate Sensitivity, Geophys. Monogr. Ser.*, vol. 29, edited by J. E. Hansen and T. Takahashi, pp. 130–163, AGU, Washington, D. C.

Hansen, J., M. Sato, and R. Ruedy (1997), Radiative forcing and climate response, *J. Geophys. Res.*, *102*, 6831–6864.

Hansen, J., et al. (2005), Efficacy of climate forcings, *J. Geophys. Res.*, *110*, D18104, doi:10.1029/2005JD005776.

Hogrefe, C., J. Biswas, B. Lynn, K. Civerolo, J.-Y. Ku, J. Rosenthal, C. Rosenzweig, R. Goldberg, and P. L. Kinney (2004), Simulating regional-scale ozone climatology over the eastern United States: Model evaluation results, *Atmos. Environ.*, *38*, 2627–2638.

Holzer, M., and G. J. Boer (2001), Simulated changes in atmospheric transport climate, *J. Clim.*, *14*, 4398–4420.

Intergovernmental Panel on Climate Change (IPCC) (1995), *C*limate Change 1995, edited by J. T. Houghton et al., Cambridge Univ. Press, New York.

Intergovernmental Panel on Climate Change (IPCC) (2001), *Climate Change 2001*, edited by J. T. Houghton et al., Cambridge Univ. Press, New York.

Iversen, T., and Ø. Seland (2002), A scheme for process-tagged SO4 and BC aerosols in NCAR CCM3: Validation and sensitivity to cloud processes, *J. Geophys. Res.*, *107*(D24), 4751, doi:10.1029/2001JD000885.

Johnson, C. E., W. J. Collins, D. S. Stevenson, and R. G. Derwent (1999), Relative roles of climate and emissions changes on future tropospheric oxidant concentrations, *J. Geophys. Res.*, *104*, 18,631–18,645.

Johnson, C. E., D. S. Stevenson, W. J. Collins, and R. G. Derwent (2001), Role of climate feedback on methane and ozone studied with a coupled Ocean-Atmosphere-Chemistry model, *Geophys. Res. Lett.*, *28*(9), 1723–1726.

Kalnay, E., et al. (1996), The NCEP/NCAR 40–year reanalysis project, *Bull. Am. Meteorol. Soc.*, *77*, 437–471.

Kanakidou, M., K. Tsigaridis, F. J. Dentener, and P. J. Crutzen (2000), Human activity-enhanced formation of organic aerosols by biogenic hydrocarbon oxidation, *J. Geophys. Res.*, *105*, 9243–9254.

Kettle, A. J., et al. (1999), A global database of sea surface dimethylsulfide (DMS) measurements and a procedure to predict sea surface DMS as a function of latitude, longitude and month, *Global Biogeochem. Cycles*, *13*, 399–444.

Kiehl, J. T., C. A. Shields, J. J. Hack, and W. D. Collins (2006), The climate sensitivity of the Community Climate System Model: CCSM3, *J. Clim.*, in press.

Koch, D. M. (2001), Transport and direct radiative forcing of carbonaceous and sulfate aerosols in the GISS GCM, *J. Geophys. Res.*, *106*, 20,311–20,332.

Lathière, J., D. A. Hauglustaine, N. De Noblet-Ducoudré, G. Krinner, and G. A. Folberth (2005), Past and future changes in biogenic volatile organic compound emissions simulated with a global dynamic vegetation model, *Geophys. Res. Lett.*, *32*, L20818, doi:10.1029/2005GL024164.

Liao, H., and J. H. Seinfeld (1998), Effect of clouds on direct aerosol radiative forcing of climate, *J. Geophys. Res.*, *103*, 3781–3788.

Liao, H., and J. H. Seinfeld (2005), Global impacts of gas-phase chemistry-aerosol interactions on direct radiative forcing by anthropogenic aerosols and ozone, *J. Geophys. Res.*, *110*, D18208, doi:10.1029/2005JD005907.

Liao, H., P. J. Adams, S. H. Chung, J. H. Seinfeld, L. J. Mickley, and D. J. Jacob (2003), Interactions between tropospheric chemistry and aerosols in a unified general circulation model, *J. Geophys. Res.*, *108*(D1), 4001, doi:10.1029/2001JD001260.

Liao, H., J. H. Seinfeld, P. J. Adams, and L. J. Mickley (2004), Global radiative forcing of coupled tropospheric ozone and aerosols in a unified general circulation model, *J. Geophys. Res.*, *109*, D16207, doi:10.1029/2003JD004456.

Liousse, C., J. E. Penner, C. Chuang, J. J. Walton, H. Eddleman, and H. Cachier (1996), A global three-dimensional model study of carbonaceous aerosols, *J. Geophys. Res.*, *101*, 19,411–19,432.

Liss, P., and L. Merlivat (1986), Air–sea gas exchange: Introduction and synthesis, in *The Role of Air–Sea Exchange in Geochemical Cycling*, edited by P. Buat-Ménard, pp. 113–127, Springer, New York.

Mickley, L. J., P. Murti, D. Jacob, J. Logan, and D. Rind (1999), Radiative forcing from tropospheric ozone calculated with a unified chemistry-climate model, *J. Geophys. Res.*, *104*, 30,153–30,172.

Mickley, L. J., D. J. Jacob, B. D. Field, and D. Rind (2004), Climate response to the increase in tropospheric ozone since preindustrial times: A comparison between ozone and equivalent CO_2 forcings, *J. Geophys. Res.*, *109*, D05106, doi:10.1029/2003JD003653.

Mitchell, J. F. B. (1989), The ''greenhouse'' effect and climate change, *Rev. Geophys.*, *27*, 115–139.

Monahan, E. C., D. E. Spiel, and K. L. Davidson (1986), A model of marine aerosol generation via whitecaps and wave disruption, in *Oceanic Whitecaps and Their Role in Air-Sea Exchange*, edited by E. C. Monahan and G. MacNiocaill, pp. 167–174, Springer, New York.

Murazaki, K., and P. Hess (2006), How does climate change contribute to surface ozone change over the United States?, *J. Geophys. Res.*, *111*, D05301, doi:10.1029/2005JD005873.

Nenes, A., C. Pilinis, and S. N. Pandis (1998), Isorropia: A new thermodynamic equilibrium model for multiphase multicomponent inorganic aerosols, *Aquat. Geochem.*, *4*, 123–152.

Penner, J. E., H. Eddleman, and T. Novakov (1993), Towards the development of a global inventory for black carbon emissions, *Atmos. Environ. Part A*, *27*, 1277–1295.

P'etron, G., P. Harley, J. Greenberg, and A. Guenther (2001), Seasonal temperature variations influence isoprene emission, *Geophys. Res. Lett.*, *28*, 1707–1710.

Ramaswamy, V. (2001), Radiative forcing of climate change, in *Climate Change 2001: The Scientific Basis. Contribution of Working Group I to the Third Assessment Report of the Intergovernmental Panel on Climate Change*, pp. 349–416, Cambridge Univ. Press, New York.

Rind, D., and J. Lerner (1996), The use of on-line tracers as a diagnostic tool in general circulation model development, 1, Horizontal and vertical transport in the troposphere, *J. Geophys. Res.*, *101*, 12,667–12,683.

Rind, D., and W. Rossow (1984), The effects of physical processes on the Hadley circulation, *J. Atmos. Sci.*, *41*, 479–507.

Rind, D., R. Suozzo, N. K. Balachandran, and M. Prather (1990), Climate change and the middle atmosphere, 1, The doubled CO_2 climate, *J. Atmos. Sci.*, *47*, 475–494.

Rind, D., D. Shindell, P. Lonergan, and N. K. Balachandran (1998), Climate change and the middle atmosphere, III, The doubled CO_2 climate revisited, *J. Clim.*, *11*, 876–894.

Rind, D., J. Lerner, K. Shah, and R. Suozzo (1999), Use of on-line tracers as a diagnostic tool in general circulation model development, 2, Transport between the troposphere and stratosphere, *J. Geophys. Res.*, *104*, 9151–9167.

Rind, D., J. Lerner, and C. McLinden (2001), Changes of tracer distribution in the doubled CO_2 climate, *J. Geophys. Res.*, *106*, 28,061–28,080.

Rosenstiel, T. N., M. J. Potosnak, K. L. Griffin, R. Fall, and R. K. Monson (2003), Increased CO_2 uncouples growth from isoprene emission in an agriforest ecosystem, *Nature*, *421*(6920), 256–259.

Russell, G. L., J. R. Miller, and L.-C. Tsang (1984), Seasonal ocean heat transports computed from an atmospheric model, *Dyn. Atmos. Oceans*, *9*, 253–271.

Sanderson, M. G., C. D. Jones, W. J. Collins, C. E. Johnson, and R. G. Derwent (2003), Effect of climate change on isoprene emissions and surface ozone levels, *Geophys. Res. Lett.*, *30*(18), 1936, doi:10.1029/2003GL017642.

Sinha, A., and R. Toumi (1997), Tropospheric ozone, lightning, and climate change, *J. Geophys. Res.*, *102*, 10,667–10,672.

Smith, K. H., and N. M. Harrison (1998), The sea spray generation function, *J. Aerosol Sci.*, *29*, suppl. 1, S189–S190.

Stevenson, D. S., R. M. Doherty, M. G. Sanderson, C. E. Johnson, W. J. Collins, and R. G. Derwent (2005), Impacts of climate change and variability on tropospheric ozone and its precursors, *Faraday Discuss.*, *130*, doi:10.1039/b417412g.

Sudo, K., M. Takahashi, and H. Akimoto (2003), Future changes in stratosphere-troposphere exchange and their impacts on future tropospheric ozone simulations, *Geophys. Res. Lett.*, *30*(24), 2256, doi:10.1029/2003GL018526.

Toumi, R., J. D. Haigh, and K. S. Law (1996), A tropospheric ozone-lightning climate feedback, *Geophys. Res. Lett.*, *23*, 1037–1040.

Wang, Y., D. J. Jacob, and J. A. Logan (1998), Global simulation of tropospheric O_3-NO_x-hydrocarbon chemistry: 1. Model formulation, *J. Geophys. Res.*, *103*, 10,713–10,726.

Wesely, M. L. (1989), Parameterization of surface resistances to gaseous dry deposition in regional-scale numerical models, *Atmos. Environ.*, *23*, 1293–1304.

Yienger, J. J., and H. Levy (1995), Empirical-model of global soil-biogenic NO_x emissions, *J. Geophys. Res.*, *100*, 11,447–11,464.

Zeng, G., and J. A. Pyle (2003), Changes in tropospheric ozone between 2000 and 2100 modeled in a chemistry-climate model, *Geophys. Res. Lett.*, *30*(7), 1392, doi:10.1029/2002GL016708.

W.-T. Chen, H. Liao, and J. H. Seinfeld, Department of Environmental Science and Engineering, California Institute of Technology, Pasadena, CA 91125, USA. (seinfeld@caltech.edu)